

Photo-assisted spin transport in double quantum dots with spin-orbit interaction

David Fernández-Fernández¹, Jordi Picó-Cortés^{1,2}, Sergio Vela Liñán³ and Gloria Platero¹

¹ Instituto de Ciencia de Materiales de Madrid ICM-CONIC, 28049 Madrid, Spain

² Institute for Theoretical Physics, University of Regensburg, 93040 Regensburg, Germany

³ Universidad Complutense de Madrid, Facultad de Ciencias Físicas, 28040 Madrid, Spain

27 February 2023

Abstract. We investigate the effect of spin-orbit interaction on the intra- and interdot particle dynamics of a double quantum dot under ac electric fields. The former is modeled as an effective ac magnetic field that produces electric-dipole spin resonance transitions, while the latter is introduced via spin-flip tunneling amplitudes. We observe the appearance of non-trivial spin-polarized dark states, arising from an ac-induced interference between photo-assisted spin-conserving and spin-flip tunneling processes. These dark states can be employed to precisely measure the spin-orbit coupling in quantum dot systems. Furthermore, we show that the interplay between photo-assisted transitions and spin-flip tunneling allows the system to operate as a highly tunable spin filter. Finally, we investigate the operation of the system as a resonant flopping-mode qubit for arbitrary ac voltage amplitudes, allowing for high tunability and enhanced qubit control possibilities.

Keywords: semiconductor quantum dots, spin-orbit coupling, quantum transport, spin qubits, dark states, ac-driving dynamics and transport, electron dipole spin resonance

1. Introduction

Semiconductor spin qubits are among the most promising platforms for the implementation of quantum computing [1, 2, 3, 4, 5, 6, 7, 8]. Some of their main advantages are the long coherence times and the promise of high scalability to achieve the large number of qubits needed for the realization of quantum algorithms [9, 10, 11, 12, 13, 14]. In these systems, qubits are encoded in the spin states of electrons or holes localized in quantum dots (QDs). Manipulation of the qubit states can be performed employing electron spin resonance (ESR) [15, 16, 17, 18] by applying an oscillating magnetic field. However, the localization of the ac magnetic fields needed to address individual dots is experimentally challenging [15]. To overcome this limitation,

an effective ac magnetic field is generated by electrically driving the particle in a material with strong spin-orbit coupling (SOC) [19, 20, 21, 22, 23, 24, 25, 26, 27, 28, 29, 30], a magnetic field gradient [31, 32, 33], a spatially dependent hyperfine field [34, 35], or modulated anisotropies of the effective g -factor [36, 37, 38]. All these alternatives allow for electrical manipulation via the so-called electric-dipole spin resonance (EDSR), which in recent years has been widely employed to obtain high-fidelity one- and two-qubit gates [39, 40, 41, 42, 43, 44, 45, 46, 47].

In a double quantum dot (DQD), the particle (electron or hole) is delocalized between the two sites, giving rise to molecular-like orbitals. The addition of an ac electric or magnetic field results in unusual properties that arise from quantum coherence and, in particular, from quantum interferences. Some of the most relevant examples in QD systems are charge and spin dynamical localization [48, 49, 50, 51], spin filtering [52, 53, 54], or long-range transfer mediated by photo-assisted tunneling (PAT) [55, 56, 57]. These effects can be analyzed using Floquet theory [58, 59, 60], which is an excellent tool for addressing time-periodic Hamiltonians. Although all of these phenomena have been widely studied both theoretically and experimentally, the consequences of adding a strong SOC have only begun to be extensively analyzed in recent years [61, 62, 63, 64]. In particular, the transport signatures under both strong SOC and large ac voltage amplitudes have not been widely investigated.

Transport through such a system is characterized by a spin-polarized current due to the finite probability of spin-flip tunneling between states of opposite spin in different QDs. In the presence of an ac electric field, these transitions can occur with the absorption or emission of one or more photons. We analyze the current and spin polarization through the system, including the effect of excited states via an effective magnetic field. Furthermore, within a certain parameter configuration, we find a set of non-trivial dark states (DS) in which the interference between PAT spin-conserving and spin-flip transitions occurs. These processes yield a complex and nonlinear current output with remarkable features, including a potential read-out mechanism of the SOC. Lastly, we consider the possibility of employing the setup as a flopping-mode qubit, in which virtual transitions between the QDs in the presence of a strong SOC allow for fully coherent manipulation of the spin. The flopping-mode qubit has recently gained attention as a promising platform for quantum computing in solid-state systems [65, 66, 67].

2. Theoretical framework

We consider the following Hamiltonian for the DQD ($\hbar = 1$)

$$\hat{H}(t) = \hat{H}_0(t) + \hat{H}_1(t), \quad (1a)$$

$$\hat{H}_0(t) = \sum_{\eta;\sigma} \epsilon_{\eta}(t) \hat{d}_{\eta,\sigma}^{\dagger} \hat{d}_{\eta,\sigma} + \sum_{\eta} \frac{E_z}{2} \hat{\sigma}_{z,\eta} \quad (1b)$$

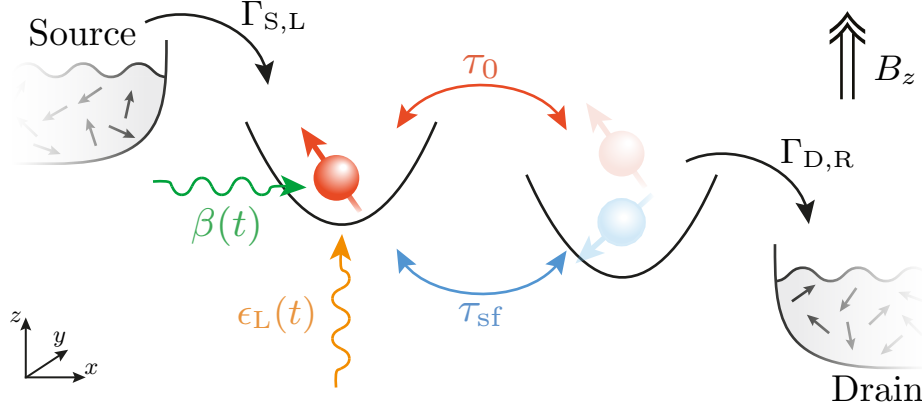


Figure 1. Schematic picture of a DQD in the x-y plane, connected to unpolarized contacts. Particles can enter through the left lead and exit to the right one with tunneling rates $\Gamma_{S,L}$ and $\Gamma_{D,R}$, respectively. A uniform magnetic field is applied pointing in the z-direction. The particle can tunnel between QDs following a spin-conserving path τ_0 . Additionally, due to the SOC, a spin-flip tunneling τ_{sf} is also present. Finally, an ac electric field is applied to the left gate $\epsilon_L(t)$, which in combination with the SOC gives rise to the OME term $\beta(t)$ (see text).

$$\begin{aligned}
 & + \sum_{\eta \neq \eta'; \sigma, \sigma'} \tau_{\eta, \sigma; \eta', \sigma'} \left(\hat{d}_{\eta, \sigma}^\dagger \hat{d}_{\eta', \sigma'} + h.c. \right), \\
 \hat{H}_1(t) = & \sum_{\eta} \frac{\beta_{\eta}(t)}{2} \hat{\sigma}_{x, \eta},
 \end{aligned} \tag{1c}$$

where $\hat{d}_{\eta, \sigma}$ ($\hat{d}_{\eta, \sigma}^\dagger$) is the annihilation (creation) operator at site $\eta \in \{L, R\}$, with spin $\sigma \in \{\uparrow, \downarrow\}$. The first term in \hat{H}_0 represents the QD energy levels $\epsilon_{\eta}(t)$, which can be controlled by electric gates applied to individual dots. We consider a sinusoidal time-dependent gate in the leftmost dot: $\epsilon_{\eta}(t) = \epsilon_{\eta, 0} + \epsilon_{ac} \cos(\omega t) \delta_{\eta, L}$. The second term is the Zeeman splitting $E_z = g\mu_B B_z$, due to the external magnetic field B applied perpendicularly to the QDs plane. The third term represents the hopping between dots. We consider two possible tunneling paths: a spin-conserving path $\propto \delta_{\sigma, \sigma'}$ of amplitude τ_0 and a spin-flip path with $\sigma \neq \sigma'$ of amplitude τ_{sf} that arises due to the SOC. The direction of the SOC determines the form of the spin-flip tunneling term. Using the SOC vector [68, 66] α , the spin-flip term is $\propto \alpha \cdot \hat{\sigma}$. Here, without loss of generality, we consider α in the y-direction, such that $\tau_{sf} \in \mathbb{R}$ (see Appendix A). Note that we have not included a Coulomb interaction term as we will focus on the single-particle dynamics.

The Hamiltonian above does not explicitly include excited states of the QD confining potential. However, in combination with the SOC and an ac electric field, the intra-dot dynamics result in the appearance of an effective magnetic field [69], as employed for the manipulation of spin qubits in EDSR protocols. In the present model, this effective magnetic field is contained in $\hat{H}_1(t)$. We derive this term in the context of a Schrieffer-Wolff transformation (SWT) in Appendix A. Under SOC, inter- and intra-dot

dynamics yield distinct contributions to the spin motion [70]. Hence, we will refer to this term as the orbital magneto-electric effect (OME) in order to distinguish it from the similar effective magnetic field that arises due to the inter-dot dynamics of the spin, which we refer to as the tunneling magneto-electric effect (TME). This effect appears as a result of a finite spin-flip tunneling amplitude, and we discuss it in more detail in section 5.

The OME is orthogonal to the SOC vector and therefore we consider it along the x-direction. Moreover, for a homogeneous electric field along the axis of the DQD, the OME term is the same in both dots $\beta_L(t) = \beta_R(t) = \beta(t)$. Here, we consider $\beta(t) = \beta_{\text{SO}} \cos(\omega t)$, with $\beta_{\text{SO}} \in \mathbb{R}$. Note that the frequency of the OME term is the same as $\epsilon_L(t)$, as it arises from the same applied voltage. The static contribution to the electric field produces only a negligible rotation of the spin axis, and we disregard this effect in the following (see Appendix A). Finally, we remark that the OME term appears only for $E_z \neq 0$, which is needed to break time-reversal symmetry. In the case where E_z is small, the hyperfine interaction may produce an equivalent effect [69].

The total Hamiltonian, written on the basis $\{|L \uparrow\rangle, |L \downarrow\rangle, |R \uparrow\rangle, |R \downarrow\rangle\}$, reads

$$\hat{H} = \begin{pmatrix} \epsilon_L(t) + E_z/2 & \beta(t)/2 & -\tau_0 & -\tau_{\text{sf}} \\ \beta(t)/2 & \epsilon_L(t) - E_z/2 & \tau_{\text{sf}} & -\tau_0 \\ -\tau_0 & \tau_{\text{sf}} & \epsilon_R + E_z/2 & \beta(t)/2 \\ -\tau_{\text{sf}} & -\tau_0 & \beta(t)/2 & \epsilon_R - E_z/2 \end{pmatrix}. \quad (2)$$

We consider the following parameter to characterize the relationship between the spin-conserving and spin-flip tunneling amplitudes

$$\chi \equiv \frac{1}{\tau_0/\tau_{\text{sf}} + 1}, \quad (3)$$

so that $\chi = 0$ corresponds to $\tau_{\text{sf}} = 0$, and $\chi = 1$ to $\tau_0 = 0$. We normalize the tunneling rates so that $\tau_0 + \tau_{\text{sf}} = \tau$. Most systems exhibit a spin-flip contribution to tunneling that is much smaller compared to the spin-conserving one [71]. However, an applied external field can be employed to tune the SOC and therefore the spin-flip contribution, e.g., in GaAs-based hole QDs [72, 73]. Spin polarization in the external leads can further produce synthetic SOC in DQDs [74]. Therefore, we investigate arbitrary values of χ in the following.

Current readout is performed by coupling the QD chain to a source (S) and drain (D) leads. The coupling between the leads and the QD chain is given by

$$\hat{H}_\Gamma = \sum_{l, \mathbf{k}, \sigma, \eta} (\gamma_{l, \eta} \hat{c}_{l, \mathbf{k}, \sigma}^\dagger \hat{d}_{\eta, \sigma} + h.c.), \quad (4)$$

with $\hat{c}_{l, \mathbf{k}, \sigma}$ the annihilation operator for a particle in the lead $l = \{S, D\}$, with spin σ and momentum \mathbf{k} . We consider the coupling between the leads and the QD chain to be spin-conserving. We further consider the infinite bias limit, so that transport is unidirectional from source to drain. Additionally, in this limit, all the side-bands couple equally to the source lead. Thus, following the property of the Bessel functions

$\sum_n J_n(\epsilon_{ac}/\omega)^2 = 1$, we can neglect the effect of the renormalization of $\gamma_{l,\eta}$ due to the ac electric field [55].

We consider the dynamics of the system via its reduced density matrix $\hat{\rho}(t)$, which, under a Markovian approximation, satisfies the master equation

$$i\frac{d}{dt}\hat{\rho}(t) = [\hat{H}(t), \hat{\rho}(t)] + \mathcal{K}\hat{\rho}(t), \quad (5)$$

where

$$\begin{aligned} \mathcal{K}\hat{\rho} = \sum_{\sigma} \left[\Gamma_{S,L} \left(\hat{d}_{L,\sigma}^{\dagger} \hat{\rho} \hat{d}_{L,\sigma} - \frac{1}{2} \left\{ \hat{d}_{L,\sigma} \hat{d}_{L,\sigma}^{\dagger}, \hat{\rho} \right\} \right) \right. \\ \left. + \Gamma_{D,R} \left(\hat{d}_{R,\sigma} \hat{\rho} \hat{d}_{R,\sigma}^{\dagger} - \frac{1}{2} \left\{ \hat{d}_{R,\sigma}^{\dagger} \hat{d}_{R,\sigma}, \hat{\rho} \right\} \right) \right], \end{aligned} \quad (6)$$

is the kernel superoperator for weak coupling in the infinite bias approximation. Transition rates due to coupling with leads are defined as $\Gamma_{l,\eta} = 2\pi/|\gamma_{l,\eta}|^2 D_l(\epsilon_F)$, where $D_l(\epsilon)$ is the density of states of the lead l and ϵ_F is the Fermi energy. We consider the case of strongly interacting QDs, where the energy difference between the single- and double-occupied states is much larger than that of the rest of the energy scales of the system, allowing us to investigate charge transport in the single-charge section of the stability diagram.

The steady-state current can then be calculated as

$$I^{\infty} = e \sum_{\sigma} \Gamma_{D,R} \rho_{R\sigma}^{\infty}, \quad (7)$$

where

$$\rho_{R\sigma}^{\infty} = \lim_{t \rightarrow \infty} \frac{1}{T} \int_t^{t+T} ds \langle R\sigma | \hat{\rho}(s) | R\sigma \rangle, \quad (8)$$

is the occupation of the rightmost dot with spin σ in the stationary state averaged over one period $T = 2\pi/\omega$ of the ac voltage. In the following, we consider an identical coupling to both leads, so that $\Gamma_{S,L} = \Gamma_{D,R} = \Gamma$.

3. Quantum transport in DQD with spin-orbit interaction

In the case where $E_z \sim 0$, quantum transport occurs only close to zero detuning $\delta \equiv \epsilon_{R,0} - \epsilon_{L,0} = 0$, where the levels of the two dots are aligned. The presence of an ac field changes this picture by allowing for PAT in which the particle can tunnel from one dot to the other one by absorbing or emitting a certain number of photons. Then, an n -photon resonance occurs for $\delta = n\omega$, $n \in \mathbb{Z}$.

For $E_z \neq 0$, the degeneracy of the spin doublets is broken, resulting in a current that will generally be spin polarized. Then, we can distinguish several processes, schematized in figure 2. First, spin-conserving resonances with either no photons (process 1), also known as direct resonance, or with the emission/absorption of a photon (process 4). As in the case without a magnetic field, these occur at $\delta = n\omega$, in which the particle can tunnel directly from one dot to the other. These resonances survive the presence

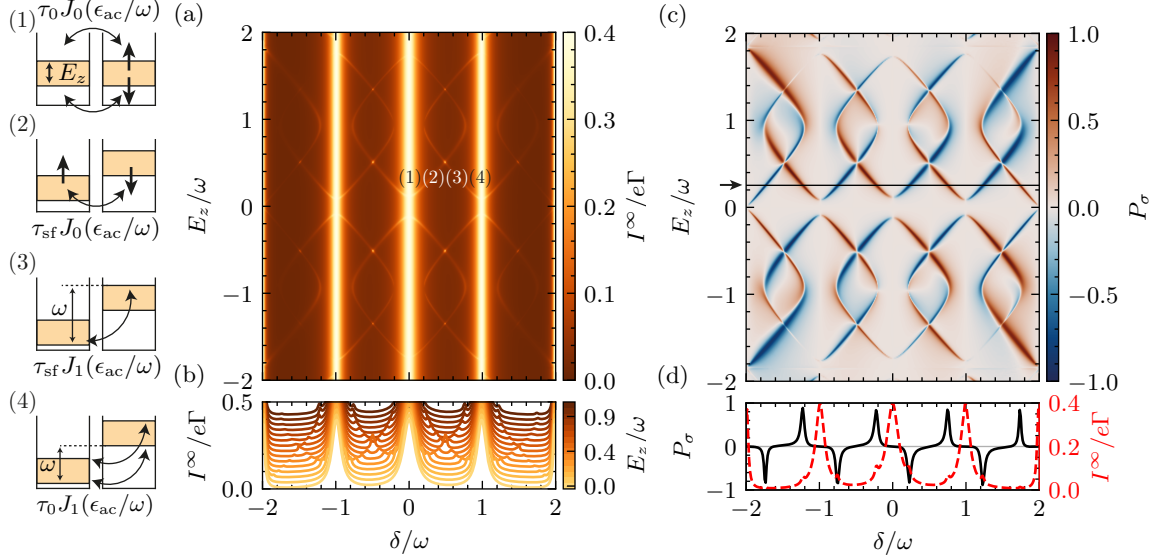


Figure 2. (a) Current through a DQD as a function of δ and E_z for $\chi = 0.1$ and $\beta_{\text{SO}} = E_z/2$. Highlighted in the figure, there is a set of four characteristic processes numbered 1 – 4. Process 1 corresponds to direct spin-conserving PAT through the two spin channels at $\delta = 0$. Process 2 corresponds to direct spin-flip PAT. Process 3 corresponds to spin-flip PAT involving one photon. Process 4 corresponds to spin-conserving PAT involving one photon through the two spin channels at $\delta = \omega$. All four processes are schematically represented on the left side of the figure. (b) A set of cuts in panel (a) at different values of E_z , with a small offset of the y -axis for clarity. (c) Spin polarization of the current as a function of δ and E_z . (d) Spin polarization (solid black, left axis) and total current (dashed red, right axis) for $E_z = 0.25\omega$ as a function of δ , represented by the horizontal cut in panel (c). In regions around $\delta = \pm 0.5\omega$, the current can be switched directly from one polarization to the opposite one with comparable intensity. Other parameters are $\omega = 10\tau = 100\Gamma$, and $\epsilon_{\text{ac}} = 1.2\omega$.

of a magnetic field, since the difference in energy between one particle with the same spin in different dots is also δ . Moreover, since the levels are now split in spin by the magnetic field, there can also be resonances when the states with opposite spin have the same energy, which is enabled by the presence of a spin-flip component in the tunneling amplitudes. This will occur whenever $\delta = \pm E_z$, as represented in figure 2 (process 2). Moreover, in the presence of an ac bias, these resonances are accompanied by a set of replicas due to PAT. This is process 3 in figure 2. As a result, when the current is represented as a function of δ and E_z as in figure 2(a), we find both the usual resonances at $\delta = n\omega$ and a set of spin-flip resonances along the lines

$$\delta + n\omega = \pm E_z. \quad (9)$$

In the $\delta - E_z$ representation of figure 2(a), these correspond *mostly* to diagonal lines. Note that transport at these resonances is not blocked when a particle tunnels from the source into the left dot with a direction that is not energy-aligned with any state on the right dot (such as $|L \downarrow\rangle$ in process 2 of figure 2). Due to the finite spin-flip tunneling

amplitude, the spin states always have a small component of the opposite spin. Another way to see this is that the spin rotates as a result of virtual tunneling to the dot via the aforementioned TME until it aligns with the resonance.

However, there are several points where this simple picture breaks down. In the vicinity of a PAT process with n photons the states in the two dots are strongly hybridized with energies

$$E_{\pm} = \delta \pm \tau J_n \left(\frac{\epsilon_{ac}}{\omega} \right), \quad (10)$$

for the two molecular states, where $J_n(z)$ is the n th-order Bessel function. There, the diagonal lines are no longer straight but curve at $E_z \approx \pm\tau$, corresponding to the resonance conditions with the energies given by equation (10). This is clearly seen in figure 2(a) in the PAT resonances near $E_z = 0$. The overall shape of these resonances closely follows hyperbolas in the $\delta - E_z$ representation shown there.

Another departure from this simple picture occurs near $E_z = \pm\omega$, where the OME field induces resonant transitions between the two spin states. There, the spin-flip resonances do not cross the spin-conserving PAT resonances at $\delta = \pm\omega$. Instead, the spin-flip resonant lines are *repelled* so that a current-free gap opens between the main resonances (1) and the spin-flip resonances (2). Moreover, we see another effect on the current at the main resonances at $\delta = 0$. There, the spin-flip resonances cross the main resonances at $E_z = \pm(\tau + \beta_{SO})$ instead of simply crossing at $E_z = \pm\tau$, as discussed above. The spin-flip resonances are then still hyperbolas but vertically displaced from where they would be for $\beta_{SO} = 0$. Finally, when photo-assisted spin-flip resonances with zero or one photon meet, they do not get distorted (such as at $\delta = \pm\omega/2$, $E_z = \pm\omega/2$ in figure 2(a)) as they correspond to processes that transmit different spin polarizations.

The spin polarization of the current is defined as

$$P_{\sigma} = \frac{I_{\uparrow}^{\infty} - I_{\downarrow}^{\infty}}{I_{\uparrow}^{\infty} + I_{\downarrow}^{\infty}}, \quad (11)$$

where $I_{\sigma}^{\infty} = e\Gamma\rho_{R,\sigma}^{\infty}$. We have represented P_{σ} as a function of δ and E_z in figure 2(c). As expected, the spin polarization is non-zero at the spin-flip current branches, provided that only one path is active (either $|L \uparrow\rangle \rightarrow |R \downarrow\rangle$ or $|L \downarrow\rangle \rightarrow |R \uparrow\rangle$). We are able to obtain spin polarization close to 1, with the largest limitation in this setup being the overlap of a spin-flip resonance with a spin-conserving PAT resonance. The width of spin-conserving resonances can be tuned by reducing τ_0 , and the separation between PATs can be increased by varying the ac voltage frequency ω .

This setup allows for several ways of controlling spin polarization. In figure 2(d), we show the polarization together with the total current. By varying δ from $\delta \simeq 0.2\omega$ to $\delta \simeq 0.8\omega$, we are able to shift from a direct PAT resonance with a strong spin polarization in one direction to a one-photon PAT resonance with a strong spin polarization in the opposite one. Hence, polarization can be inverted without crossing the resonance at $\delta = 0$. Since δ is often one of the easiest parameters to control in experimental setups, this allows us to generate highly tunable fully spin-polarized currents. This is remarkable, since the spin-flip amplitude in this case has been considered very small

($\chi = 0.1$). With a correct tuning of χ and τ (reducing the width of the spin-conserving resonances), the spin polarization can be adjusted to an even larger degree.

We note a slight asymmetry in the spin polarization in the two adjacent highly polarized peaks at $\delta \simeq 0.2\omega$ and $\delta \simeq 0.8\omega$ resulting from the OME term. This can be seen in figure 2(c), where the resonance lines have different widths depending on whether they cross the $E_z = \pm\omega$, $\delta = \pm\omega$ points or not. For $\beta_{\text{SO}} \rightarrow 0$, the current associated with the two resonances has the same absolute value of polarization (and is close to $P_\sigma = \pm 1$, respectively).

Tuning the frequency of the ac voltage, the setup allows another mode of generating spin-polarized currents. The DQD can be initialized in a configuration in which direct resonances without photons are energetically disfavored. Then, applying a voltage with the frequency tuned to either the spin-conserving or the spin-flip resonance with absorption or emission of photons, the resulting current will be spin-polarized in one direction or the other, depending on the spin of the initial state. Both modes of operation allow for fully electric control of the spin polarization of the current without the need to modify the magnetic fields, which enables fast control of the current under experimental conditions.

Next, we study the effect of varying the amplitude of the ac voltage. Due to Landau-Zener-Stückelberg (LZS) interferences, if the QDs are in resonance $\delta = n\omega$, photo-assisted transitions can be understood to occur with a tunneling amplitude renormalized by a Bessel function as [58, 59, 75]

$$\tau_\zeta \rightarrow \tau_\zeta J_n \left(\frac{\epsilon_{\text{ac}}}{\omega} \right), \quad \zeta \in \{0, \text{sf}\}. \quad (12)$$

Crucially, both the spin-conserving and spin-flip amplitudes are equally modified by the presence of the ac field \ddagger . This well-known expression holds except at the points where the spin levels are in resonance as well ($E_z = m\omega$), as we will see in the next sections. At the zeros of any given Bessel function, destructive interference occurs, and both spin-conserving and spin-flip tunneling rates are suppressed. This effect is known as coherent destruction of tunneling (CDT) [49]. The resulting pattern is given in figure 3(a), where we have represented the current as a function of both δ and ϵ_{ac} , for a range that includes the first five photo-assisted resonances in each direction of δ , plus the resonance at $\delta = 0$. Spin-flip resonances are visible as thinner parallel lines along the ϵ_{ac} axis, two to each side of the main resonances. We have also represented in figure 3(a) (bottom panel) a set of cuts at $\epsilon_{\text{ac}} = 0$ (green), $\epsilon_{\text{ac}} = 3\omega$ (blue) and $\epsilon_{\text{ac}} = 6\omega$ (red), showing the resonance pattern (similarly to figure 2). Furthermore, figure 3(a) (left panel) shows the interference pattern that leads to CDT. Here, we have represented a set of cuts at values of $\delta = n\omega$ for $n = 0$ (pink), $n = 1$ (lime) and $n = 2$ (cyan). We also include dashed lines to denote the first zeros of $J_n(\epsilon_{\text{ac}}/\omega)$, which coincide precisely with the dips in the current at $\delta = n\omega$. Finally, in figure 3(b) we plot the spin polarization for the LZS interferometry. The main spin-conserving resonances have an unpolarized spin current $P_\sigma \sim 0$, since both the spin-up and spin-down channels are present with the

\ddagger Note that this was already taken into account in equation (10).

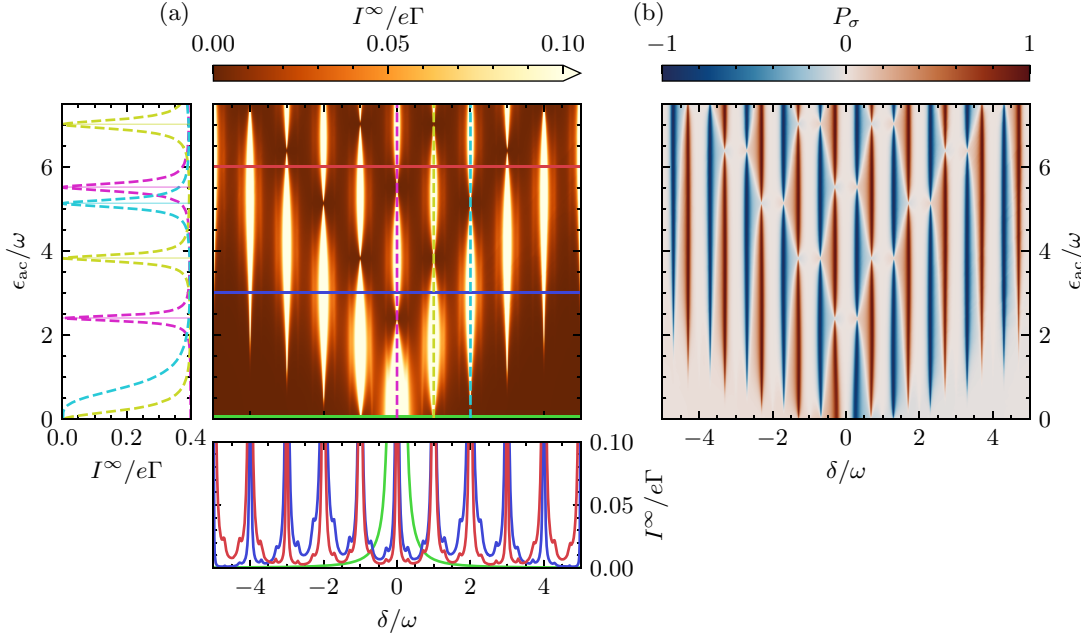


Figure 3. (a) Current and (b) spin polarization through a DQD as a function of δ and ϵ_{ac} . (a, bottom) Cuts along the horizontal axis at $\epsilon_{ac} = 0$ (green), $\epsilon_{ac} = 3\omega$ (blue), and $\epsilon_{ac} = 6\omega$ (red), showing the appearance of satellite peaks close to the main resonances for $\epsilon_{ac} \neq 0$. (a, left) Cut the along the vertical axis (dashed lines) at $\delta = n\omega$ with $n = 0$ (pink), $n = 1$ (lime), and $n = 2$ (cyan), showing the appearance of coherent destruction of tunneling, where the current drops to zero. The horizontal solid lines denote the zeros of the Bessel function $J_n(\epsilon_{ac}/\omega)$. The parameters used are $\omega = 10\tau = 100\Gamma$, $E_z = 0.3\omega$, $\beta_{SO} = 0$, and $\chi = 0.2$.

same probability. However, spin-flip resonances at $\delta = n\omega \pm E_z$ are highly spin polarized $P_\sigma \sim \pm 1$, as already mentioned above. These resonances, similar to the spin-conserving ones, also exhibit a CDT effect where $J_n(\epsilon_{ac}/\omega) = 0$.

3.1. Effect of the OME

In this section, we consider in detail the effect of the OME term. This will be, in general, a weak effect because the amplitude of the SOC-induced OME field is smaller than the electric voltage amplitude. However, as anticipated above, the OME has a strong effect near the spin resonances at $E_z \simeq n\omega$. At these points, the effective ac magnetic field can induce resonant transitions between the two spin states on the same QD. To focus on this regime, let us consider the Hamiltonian at any such resonance. We perform the following unitary transformation

$$\hat{U}(t) = \exp\left(\frac{-in\omega t \hat{\sigma}_z}{2}\right) \exp\left(\frac{-i\epsilon_{ac} \sin(\omega t)(1 + \hat{\tau}_z)}{2\omega}\right), \quad (13)$$

where $\hat{\tau}_i$ are Pauli matrices associated to the charge (left/right dot) degree of freedom. The leftmost operator transforms the system into the rotating frame at the spin resonance. The rightmost operator transforms into the interacting picture with respect

to the ac voltage, removing the corresponding term from the Hamiltonian at the cost of turning the tunneling time-dependent. Its purpose is to allow for arbitrary ac voltage amplitudes within a rotating-wave approximation (RWA) [60], under which we will work.

When the transformation of equation (13) is performed and the Jacobi-Anger expansion is employed, the terms in the Hamiltonian are changed as

$$\langle \eta\sigma | \hat{H}_0 | \eta\sigma \rangle = E_z \rightarrow E_z - n\omega, \quad (14a)$$

$$\langle R\sigma | \hat{H}_0 | L\sigma \rangle = \tau_0 \rightarrow \tau_0 \sum_{k=-\infty}^{\infty} J_k\left(\frac{\epsilon_{ac}}{\omega}\right) e^{ik\omega t}, \quad (14b)$$

$$\langle R\uparrow(\downarrow) | \hat{H}_0 | L\downarrow(\uparrow) \rangle = \pm\tau_{sf} \rightarrow \pm\tau_{sf} \sum_{k=-\infty}^{\infty} J_k\left(\frac{\epsilon_{ac}}{\omega}\right) e^{i(k\mp n)\omega t}, \quad (14c)$$

$$\langle \eta\uparrow | \hat{H}_1 | \eta\downarrow \rangle = \beta(t) \rightarrow \frac{\beta_{SO}}{2} (e^{i(n+1)\omega t} + e^{i(n-1)\omega t}). \quad (14d)$$

Other terms are obtained by imposing hermiticity on the effective Hamiltonian. Let us now consider the avoided crossing at $\delta \approx 0$, $n = 1$, visible in figure 2 (the resonance $n = -1$ follows a similar behavior). We apply now the RWA, neglecting the time-dependent terms. This yields

$$\hat{H}_{RWA} = \begin{pmatrix} -\delta/2 & \beta_{SO}/4 & -\tau_0^{RWA} & -\tau_{sf}^{RWA} \\ \beta_{SO}/4 & -\delta/2 & -\tau_{sf}^{RWA} & -\tau_0^{RWA} \\ -\tau_0^{RWA} & -\tau_{sf}^{RWA} & \delta/2 & \beta_{SO}/4 \\ -\tau_{sf}^{RWA} & -\tau_0^{RWA} & \beta_{SO}/4 & \delta/2 \end{pmatrix}, \quad (15)$$

where $\tau_0^{RWA} = \tau_0 J_0(\epsilon_{ac}/\omega)$ and $\tau_{sf}^{RWA} = \tau_{sf} J_1(\epsilon_{ac}/\omega)$. Note that at the resonance between the two spin levels, the spin-conserving tunneling amplitude is renormalized by $J_0(z)$ while the spin-flip amplitude is renormalized by $J_1(z)$, with $z = \epsilon_{ac}/\omega$.

In this frame, the OME term acts as a constant magnetic field, resulting in a splitting $\beta_{SO}/2$ of the spins in the x-direction. The avoided crossing between the spin-conserving and spin-flip resonances discussed above can be understood in this picture as the OME term producing a splitting between the spins that is only strong near the EDSR. Therefore, resonant transport occurs now when $\delta = \pm\beta_{SO}/2$. These new resonances are visible in figure 4(a) as side peaks next to the main resonance at $\delta = 0$. Note that the position of the resonances shows a linear relationship between detuning and β_{SO} , as expected. However, around $\beta_{SO} \lesssim \tau$ the hybridization between states is large enough to distort this simple picture (in the same way as for equation (10)).

The previous results are valid provided that $\beta_{SO}/\omega \ll 1$, as required by the RWA. We can further relax this condition by performing the transformation

$$\hat{U}'(t) = \exp\left(\frac{-i\beta_{SO} \sin(\omega t) \hat{\sigma}_x}{2\omega}\right) \quad (16)$$

to the original Hamiltonian in equation (2), and then apply $\hat{U}(t)$ given in equation (13). This transformation removes $\hat{H}_1(t)$ (the OME term) at the cost of transforming the

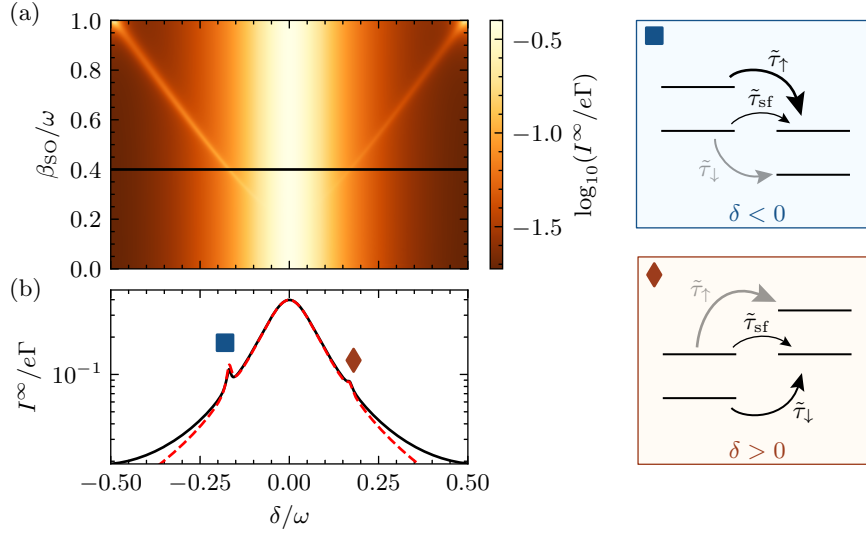


Figure 4. (a) Current through a DQD as a function of δ and β_{SO} . A cut along the horizontal axis at $\beta_{\text{SO}} = 0.4\omega$ is shown in panel (b). The black solid line is obtained with the original Hamiltonian (equation (2)), while the red dashed line is obtained by the effective Hamiltonian (equation (24)). Two satellite peaks are located at $\delta \simeq \pm\beta_{\text{SO}}/2$, marked with the blue square and red diamond symbols. The energy levels in these situations, for the effective Hamiltonian, are shown schematically on the right side of the figure. Here, the width of the arrows denotes the tunneling amplitudes for each possible path, while the gray arrows represent tunneling paths that are less favorable. In all panels, $E_z = \omega$, $\epsilon_{\text{ac}} = 1.2\omega$, $\omega = 10\tau = 100\Gamma$, and $\chi = 0.2$.

spin-flip and Zeeman splitting terms as

$$\begin{aligned} \frac{E_z}{2} \hat{\sigma}_z &\rightarrow \frac{E_z}{2} \cos \left[\frac{\beta_{\text{SO}}}{\omega} \sin(\omega t) \right] \hat{\sigma}_z \\ &+ \frac{E_z}{2} \sin \left[\frac{\beta_{\text{SO}}}{\omega} \sin(\omega t) \right] \hat{\sigma}_y, \end{aligned} \quad (17a)$$

$$\begin{aligned} \tau_{\text{sf}} \hat{\tau}_y \hat{\sigma}_y &\rightarrow \tau_{\text{sf}} \hat{\tau}_y \cos \left[\frac{\beta_{\text{SO}}}{\omega} \sin(\omega t) \right] \hat{\sigma}_y \\ &- \tau_{\text{sf}} \hat{\tau}_y \sin \left[\frac{\beta_{\text{SO}}}{\omega} \sin(\omega t) \right] \hat{\sigma}_z. \end{aligned} \quad (17b)$$

The first term on the right-hand side of the expression for E_z reflects the renormalization effect due to the ac magnetic field. Compared to equation (15), this term renormalizes the Zeeman splitting by a factor $J_0(\beta_{\text{SO}}/\omega)$. At destructive interferences where $J_0(\beta_{\text{SO}}/\omega) = 0$, the Zeeman splitting is completely suppressed in a process known as spin locking (SL) [51]. Nonetheless, this suppression occurs for values of β_{SO} beyond those discussed in Appendix A. In general, the main effect of this renormalization is that EDSR now occurs at $E_z J_0(\beta_{\text{SO}}/\omega) = n\omega$. The second term on the expression for E_z reduces for $\beta_{\text{SO}}/\omega \ll 1$ to the (phase-shifted) OME term. At resonance $n = \pm 1$, this corresponds to the substitution

$$\frac{\beta_{\text{SO}}}{2} \rightarrow E_z J_1 \left(\frac{\beta_{\text{SO}}}{\omega} \right), \quad (18)$$

e.g., in equation (15). In the limit $\beta_{\text{SO}}/\omega \ll 1$ we recover the result of the previous section, while for $J_1(\beta_{\text{SO}}/\omega) = 0$ the effective magnetic field is suppressed in a similar way to the case discussed above where spin locking takes place. Again, this effect occurs for parameters beyond the scope of the approximations of Appendix A and we do not consider it any further.

Regarding the transformed spin-flip term, given in equation (17b), it may seem that the first term would also produce a similar Bessel function renormalization. However, the spin-flip amplitude at an arbitrary β_{SO} allows sidebands to be generated from both the ac voltage and the OME term. The combination of these sidebands yields a more complicated expression. After applying the transformation of equation (13) and expanding the first term of equation (17b) using the Jacobi-Anger expansion, we find the following:

$$\pm\tau_{\text{sf}} \rightarrow \frac{\pm\tau_{\text{sf}}}{2} \sum_{k=-\infty}^{\infty} \sum_{k'=-\infty}^{\infty} J_k\left(\frac{\epsilon_{\text{ac}}}{\omega}\right) J_{2k'}\left(\frac{\beta_{\text{SO}}}{\omega}\right) \left(e^{i(-k \mp n + 2k')\omega t} + e^{i(-k \mp n - 2k')\omega t}\right), \quad (19)$$

where \pm corresponds to the sign of the two spin channels, as in equation (2). In the RWA, we find

$$\pm\tau_{\text{sf}} \rightarrow (\mp 1)^{n+1} \tau_{\text{sf}}^{\text{RWA}}, \quad (20)$$

$$\tau_{\text{sf}}^{\text{RWA}} = \tau_{\text{sf}} \sum_{k=-\infty}^{\infty} J_{2k+n}\left(\frac{\epsilon_{\text{ac}}}{\omega}\right) J_{2k}\left(\frac{\beta_{\text{SO}}}{\omega}\right). \quad (21)$$

Finally, consider the last term on equation (17b). After applying the transformation of equation (13), we find a term $\propto |L\rangle\langle R|\hat{\sigma}_z$ with amplitude

$$\tau_{\text{sf}} \sum_{k=-\infty}^{\infty} \sum_{k'=0}^{\infty} J_k\left(\frac{\epsilon_{\text{ac}}}{\omega}\right) J_{2k'+1}\left(\frac{\beta_{\text{SO}}}{\omega}\right) \left(e^{i(k+2k'+1)\omega t} - e^{i(k-2k'-1)\omega t}\right). \quad (22)$$

In the RWA, only the terms with $k = \pm(2k' + 1)$ contribute and we obtain the real tunneling rate

$$\tau_{\text{si}}^{\text{RWA}} = \tau_{\text{sf}} \sum_{k=-\infty}^{\infty} J_{2k+1}\left(\frac{\epsilon_{\text{ac}}}{\omega}\right) J_{2k+1}\left(\frac{\beta_{\text{SO}}}{\omega}\right). \quad (23)$$

This produces spin-conserving amplitudes of different absolute values depending on the direction of the spin, i.e., the spin-conserving tunneling of a spin-down particle occurs with a tunneling amplitude different from that of a spin-up particle. Note that this term arises only because of the combination of sidebands from both the ac voltage and the OME term, resulting in a finite static component that contributes to the Hamiltonian even in the RWA. Remarkably, both electric and magnetic sidebands arise from the same applied voltage. In that sense, this is a constructive self-interference effect, in a similar way to virtual tunneling processes that involve two PAT transitions [55, 57].

Let us now compare the results for arbitrary β_{SO} with the Hamiltonian in the $\beta_{\text{SO}} \ll \omega$ limit, equation (15). Again, let us focus on $n = 1$, $\delta \approx 0$. We diagonalize the spin subspace by performing a rotation around the y-axis by an angle

$\theta \equiv \arctan(E_z^{\text{RWA}}/\beta_{\text{SO}}^{\text{RWA}})$, where $E_z^{\text{RWA}} \equiv E_z J_0(\beta_{\text{SO}}/\omega) - \omega$ and $\beta_{\text{SO}}^{\text{RWA}} \equiv E_z J_1(\beta_{\text{SO}}/\omega)$. Finally, the effective Hamiltonian in its matrix form reads

$$\hat{H} = \begin{pmatrix} (\tilde{E}_z - \delta)/2 & 0 & -\tilde{\tau}_{\uparrow} & -\tilde{\tau}_{\text{sf}} \\ 0 & (-\tilde{E}_z - \delta)/2 & -\tilde{\tau}_{\text{sf}} & -\tilde{\tau}_{\downarrow} \\ -\tilde{\tau}_{\uparrow} & -\tilde{\tau}_{\text{sf}} & (\tilde{E}_z + \delta)/2 & 0 \\ -\tilde{\tau}_{\text{sf}} & -\tilde{\tau}_{\downarrow} & 0 & (-\tilde{E}_z + \delta)/2 \end{pmatrix}, \quad (24)$$

where we have defined the effective magnitudes as

$$\tilde{E}_z \equiv \sqrt{(E_z^{\text{RWA}})^2 + (\beta_{\text{SO}}^{\text{RWA}})^2}, \quad (25)$$

$$\tilde{\tau}_{\uparrow, \downarrow} \equiv \tau_0^{\text{RWA}} \mp [\sin(\theta)\tau_{\text{sf}}^{\text{RWA}} - \cos(\theta)\tau_{\text{si}}^{\text{RWA}}], \quad (26)$$

$$\tilde{\tau}_{\text{sf}} \equiv \cos(\theta)\tau_{\text{sf}}^{\text{RWA}} + \sin(\theta)\tau_{\text{si}}^{\text{RWA}}. \quad (27)$$

The effective model represents a DQD system in the presence of a homogeneous Zeeman splitting \tilde{E}_z , a spin-conserving tunneling rate which is different in general for the spin-up and spin-down channels $\tilde{\tau}_{\uparrow, \downarrow}$, and a spin-flip tunneling rate $\tilde{\tau}_{\text{sf}}$. The magnetic field can be simplified for $\beta_{\text{SO}} < \omega$ as $\tilde{E}_z = \beta_{\text{SO}}/2 + \mathcal{O}((\beta_{\text{SO}}/\omega)^5)$, recovering the linear relation between δ and β_{SO} for the resonant condition explained above. Note that the effective model is strictly only valid for small detuning $\delta \ll \omega$. The different spin-conserving tunneling rates $\tilde{\tau}_{\uparrow, \downarrow}$ contribute in a characteristic fashion to the current. In figure 4(a), we observe a significant asymmetry between the two secondary resonances depending on the sign of δ . As we shall see next, this asymmetry arises fundamentally due to the fact that $|\tilde{\tau}_{\uparrow}| \neq |\tilde{\tau}_{\downarrow}|$.

The two satellite peaks shown in figure 4(b) occur when the energies of two levels with opposite spin are in resonance §. This is the situation schematized in figure 4. If $\delta < 0$, the spin-down state of the left dot is in resonance with the spin-up state of the right dot and the most likely tunneling path is given by $\tilde{\tau}_{\text{sf}}$, while $\tilde{\tau}_{\downarrow}$ can be neglected at first order. Meanwhile, the spin-up energy level on the left dot is out of resonance with an energy difference given by \tilde{E}_z . However, due to $\tilde{\tau}_{\uparrow}$, there is still a small but finite probability of tunneling to the right dot [76]. In the case of $\delta > 0$, we have a similar situation, except that the non-resonant level (spin-down in this case) tunnels with an amplitude given by $\tilde{\tau}_{\downarrow}$. Using equations (21, 23) with $k = -2, -1, \dots, 2$, and the parameters used in figure 4(b), we obtain $\tilde{\tau}_{\uparrow} \simeq 0.06\omega$ and $\tilde{\tau}_{\downarrow} \simeq 0.04\omega$, and $\tilde{\tau}_{\text{sf}} \simeq 0.002\omega$. Since $\tilde{\tau}_{\uparrow} > \tilde{\tau}_{\downarrow}$ the effective model predicts a higher current for resonance at $\delta < 0$, which is in agreement with the numerical results obtained from the original Hamiltonian. In figure 4(b), we compare the current obtained both with the total Hamiltonian (equation (2)) and with the effective Hamiltonian (equation (24)), showing how the effective Hamiltonian predicts the presence of satellite peaks close to the main resonance and the asymmetry in δ .

§ Note that the spin-up and spin-down levels in the effective model are a non-trivial combination of the spin-up and spin-down levels of our original model. However, the population of the left and right dots in the effective model of equation (24) still resembles the same populations as in the original system of equation (2).

The fact that the asymmetry in δ is a consequence of $|\tilde{\tau}_\uparrow| \neq |\tilde{\tau}_\downarrow|$ can be further seen by calculating the effective magnetic field due to the TME, which is explicitly asymmetric in δ . This is shown in more detail in [Appendix C](#).

4. Dark state formation

Dark states are a well-known feature in open quantum systems, first described in the context of the optical response of electrons to laser pumping. In mesoscopic transport, a dark state refers to a steady state in which coherent interference results in a current blockade even in a situation where it would be expected to flow [77, 78, 79, 80]. In this particular setup, dark states correspond to a particle confined to the left dot, as the right dot will be immediately emptied by tunneling to the drain.

In the following, we focus on the main resonances $\delta = m\omega$, $m \in \mathbb{Z}$, where a non-zero current is expected to flow. In this case, as mentioned above, current blockade occurs due to the LZS interference pattern at the points where $J_m(\epsilon_{ac}/\omega) = 0$, yielding the aforementioned CDT. Taking into account the resonance $\delta = 0$, the current through the DQD can be suppressed if the driving amplitude verifies $J_0(\epsilon_{ac}/\omega) = 0$, which occurs close to $\epsilon_{ac} \simeq 2.4\omega$. As described above, this renormalization is the same for both the spin-conserving and spin-flip tunneling amplitudes. However, if the system is simultaneously in a configuration in which the spin states are also in resonance with the ac voltage frequency $E_z = n\omega$, the renormalization is not necessarily the same, as seen in the previous section. We focus on this case in the following.

Let us consider the Hamiltonian in the rotating frame, as in equation (15), for an n -photon resonance. First, consider $\beta_{SO} = 0$. We analyze below how the dark states are affected when including a non-zero OME term. In the case of a spin-up particle tunneling from the left to the right dot, emitting n photons, the spin-flip tunneling rate is renormalized as $\tau_{sf} \rightarrow \tau_{sf} J_{-n}(\epsilon_{ac}/\omega)$. On the other hand, if the particle tunnels from the left dot with spin down, it will absorb n photons, so that $\tau_{sf} \rightarrow \tau_{sf} J_n(\epsilon_{ac}/\omega)$. This situation is shown schematically in figure 5(a). The effective Hamiltonian under an RWA then reads

$$\hat{H}_{\text{RWA}}^{(n)} = \begin{pmatrix} 0 & 0 & -\tau_0 J_0(\epsilon_{ac}/\omega) & -\tau_{sf} J_n(\epsilon_{ac}/\omega) \\ 0 & 0 & \tau_{sf} J_{-n}(\epsilon_{ac}/\omega) & -\tau_0 J_0(\epsilon_{ac}/\omega) \\ -\tau_0 J_0(\epsilon_{ac}/\omega) & \tau_{sf} J_{-n}(\epsilon_{ac}/\omega) & 0 & 0 \\ -\tau_{sf} J_n(\epsilon_{ac}/\omega) & -\tau_0 J_0(\epsilon_{ac}/\omega) & 0 & 0 \end{pmatrix}. \quad (28)$$

Since $J_{-n}(z) = (-1)^n J_n(z)$, if the number of photons is odd, then the spin-flip term has the same sign for both spin directions. As discussed in [Appendix A](#), time-reversal symmetry imposes the requirement that the spin-flip term must be $\propto \hat{\tau}_y$, in terms of the charge Pauli matrices introduced above. This form of tunneling prohibits destructive interference between the spin-conserving and spin-flip tunneling channels. However, if the number of photons is even, the RWA Hamiltonian in equation (28) has a spin-flip term of the form $\hat{\tau}_x \hat{\sigma}_x$, which does not exhibit this protection. Instead, the combination

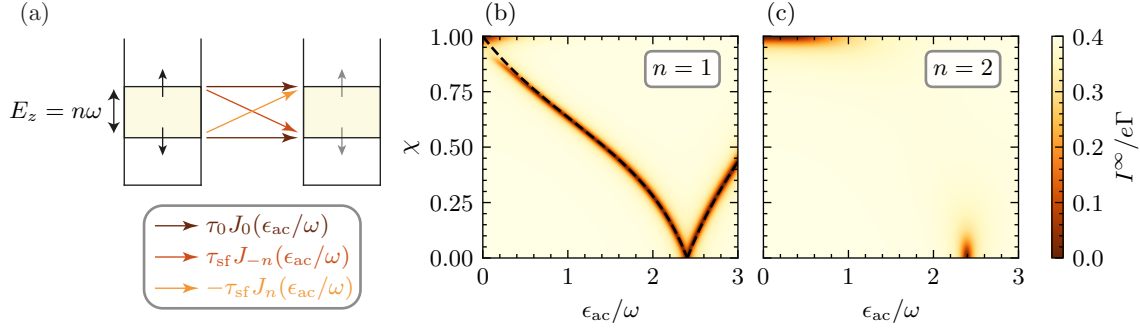


Figure 5. (a) Scheme of a DQD, with $E_z = n\omega$, and renormalized spin-conserving $\tau_0 \rightarrow \tau_0 J_0(\epsilon_{ac}/\omega)$, and spin-flip $\tau_{sf} \rightarrow \tau_{sf} J_{\pm n}(\epsilon_{ac}/\omega)$ tunneling rates. (b-c) Current through a DQD as a function of χ and ϵ_{ac} . (b) $E_z = \omega$ and (c) $E_z = 2\omega$. The dashed line represents the analytical prediction for a dark state $\tilde{\chi}^{(n)}$ (see equation (29)), which has no real solution for $n = 2$. In both cases $\delta = 0$, with $\omega = 10\tau = 100\Gamma$ and $\beta_{SO} = 0$.

of $E_z \neq 0$ (breaking time-reversal symmetry) and $\epsilon_{ac} \neq 0$ (resulting in PAT) allows the spin-conserving and spin-flip paths to interfere destructively.

By exact diagonalization of the above Hamiltonian, we look for DS of the form $|\text{DS}\rangle = (|L \uparrow\rangle + e^{i\varphi}|L \downarrow\rangle)/\sqrt{2}$ for an arbitrary relative phase φ , which we find occurs when the ratio χ between the spin-conserving and spin-flip amplitudes satisfies

$$\tilde{\chi}^{(n)} = \frac{J_0(\epsilon_{ac}/\omega)}{J_0(\epsilon_{ac}/\omega) \pm i^{n+1} J_n(\epsilon_{ac}/\omega)}, \quad (29)$$

where the superindex denotes the dependence of the dark state on the resonance with the driving $E_z = n\omega$.

Since we must impose $\tilde{\chi}^{(n)} \in \mathbb{R}$ (see equation (3)), the dark state appears only when an odd number of photons are absorbed or emitted, i.e., $n = 2k + 1$ for $k \in \mathbb{Z}$. In particular, $E_z = 0$ corresponds to taking $n = 0$, and equation (29) has no real solution showcasing the need to break the time-reversal symmetry to observe dark-state formation. The dependence on the number of photons involved in the process is known as the odd-even effect, and has already been observed in DQDs, both theoretically and experimentally [68, 81, 82, 62, 63]. This type of process is generally intrinsic to multilevel systems, in which multiple pathways destructively interfere with each other [83].

In figure 5(b-c) we show the current through a DQD in the cases of $n = 1$ and $n = 2$, respectively. In the former case, we plot the analytical prediction for the existence of a dark state, equation (29), which is in agreement with the numerical results. If the spin-conserving tunneling path is not available, i.e., $\tau_0 = 0$, or equivalently $\chi = 1$, then the only possible tunneling channel requires spin-flip, which is highly suppressed because of the large energy gap between states with opposite spin produced by E_z . This process also results in current blockade (unrelated to interference effects) and is visible in the upper left corner of this figure. For $n = 2$ we see that the only two situations where the current is suppressed coincide with $\chi \simeq 1$, $\epsilon_{ac} = 0$, and with $\chi = 0$, $\epsilon_{ac} \simeq 2.4\omega$, as expected from the even-odd effect. In an experimental situation, in which the driving amplitude

can be precisely tuned, the appearance of a sharp decrease in current at a given ϵ_{ac} can be used to determine the value of χ and hence the SOC strength. To minimize the uncertainty of the measurement, several odd resonances for $E_z = (2k + 1)\omega$ can be studied, providing a precise way to characterize the SOC present in a given device.

Next, we fix the driving amplitude at $\epsilon_{ac} = 2\omega$ and consider arbitrary values of E_z . The corresponding results are presented in figure 6(a). The DS at the exact resonant condition $E_z = \omega$ extends to non-resonant values of E_z , forming a parabola in the $E_z - \chi$ plane. Again, we perform an exact diagonalization of the RWA Hamiltonian given by equation (28) and look for dark states. Up to second order in $(E_z - \omega)$, these are found for the condition

$$\begin{aligned} \tilde{\chi}^{(1)} = & \frac{J_0(\epsilon_{ac}/\omega)^2 - |J_0(\epsilon_{ac}/\omega)J_1(\epsilon_{ac}/\omega)|}{J_0(\epsilon_{ac}/\omega)^2 - J_1(\epsilon_{ac}/\omega)^2} \\ & - \frac{(E_z - \omega)^2}{\tau^2 |J_0(\epsilon_{ac}/\omega)J_1(\epsilon_{ac}/\omega)|} + \mathcal{O}((E_z - \omega)^4). \end{aligned} \quad (30)$$

The prediction is in accordance with the numerical results (see the inset of figure 6(a)). Far from the resonance, the RWA is no longer valid, so the above equation does not apply. Once again, even if the dot levels are in resonance at $\delta = 0$, a trivial DS at $\chi = 1$ appears. In that situation, E_z is no longer in resonance with the driving, so the particle cannot absorb or emit a photon, and will be blocked in the left QD, as explained above.

Next, we consider the case for an arbitrary amplitude of the OME term. Here, we find a more complex situation. The OME term induces fast spin rotations inside the QDs, which prevents current blockade in situations where, otherwise, the particle would remain stuck in the left dot. This effect is most clearly seen in figure 6 for $\chi \simeq 1$, where the current is blocked for $\beta_{SO} = 0$ (figure 6(a)) if $E_z \neq \omega$, while for $\beta_{SO} \neq 0$ (figure 6(b)) a non-zero current can flow. Dark states, on the other hand, can still be found, now extending to all values of E_z . Interestingly, the spin projection of the steady state is highly polarized, depending on whether $0 < E_z < \omega$, for which the particle remains in the left QD with spin down, or $\omega < E_z < 2\omega$ so that the final spin projection is inverted. It is also worth mentioning that the DS obtained far from the resonance $E_z \neq \omega$ are highly pure with $\text{Tr}(\rho^2) \simeq 1$. These DSs could be used to store quantum information inside a QD without the requirement to modify the tunneling from the leads or between dots.

Due to the complexity of our system, no analytical results could be obtained for the formation of DSs for $\beta_{SO} \neq 0$. Nonetheless, we can still gain an understanding of their appearance by employing the Floquet formalism. For a T -periodic Hamiltonian, the time evolution of the wave function can be written as $|\Psi_\alpha(t)\rangle = e^{-i\varepsilon_\alpha t}|\phi_\alpha(t)\rangle$, where ε_α are the quasienergies and $|\phi_\alpha\rangle$ are the Floquet states, obtained by diagonalizing the Floquet Hamiltonian $\hat{\mathcal{H}}(t) \equiv \hat{H}(t) - i\partial_t$. According to the Von Neumann-Wigner theorem [84], crossings between distinct energy levels occur only if the corresponding states belong to different representations of the symmetry group of the system. Quasienergy crossings follow the same behavior, often signaling that the ac drive has reinstated a symmetry of the system by suppressing the relevant terms in the Hamiltonian [51]. At these

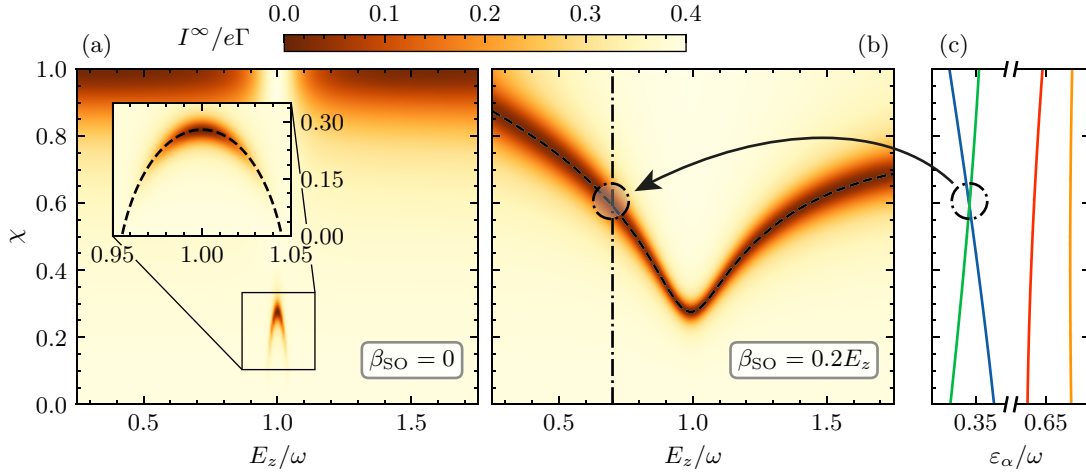


Figure 6. Current through a DQD as a function of χ and E_z for (a) $\beta_{\text{SO}} = 0$, and (b) $\beta_{\text{SO}} = 0.2E_z$. Darker colors represent the appearance of DSs. The inset in panel (a) represents a zoom into the DS around $E_z \simeq \omega$, while the dashed black line denotes the analytical prediction in equation (30). The dashed black line in panel (b) represents the DS predicted by the crossing of Floquet quasienergies. (c) Floquet quasienergies for $E_z = 0.7\omega$ (dash-dotted line, panel (b)), with the energy crossing highlighted with a circle. $\delta = 0$, $\omega = 10\tau = 100\Gamma$, $\epsilon_{\text{ac}} = 2\omega$.

crossings, the time evolution operator depends exponentially on the difference between the quasienergies. In resonance, the unitary time evolution matrix becomes the identity operator, freezing the long-term dynamics.

The quasienergies for $\beta_{\text{SO}} \neq 0$ have been obtained by means of numerical methods [85], and their crossings perfectly agree with the location of the DS found by evolving the Lindblad master equation (see figure 6(b)). The Floquet quasienergies for $E_z = 0.7\omega$ are shown in figure 6(c). The crossing is located at $\chi \simeq 0.6$, which coincides with the numerical result for the open system.

5. Flopping mode qubit operation

We next focus on the situation in which the spin motion is confined to one of the dots. Neglecting the OME term for simplicity, the spin dynamics in that case is governed by the interplay between the Zeeman splitting and the TME first discussed in section 2. In this section, we consider this regime as a possible implementation of a solid-state qubit.

Let us first consider the case where we have an electric field that is constant in time. We can perform a SWT to obtain an effective Hamiltonian for an isolated spin in one of the dots. This transformation allows us to obtain the dynamics in one energy subspace that is weakly coupled and well separated in energy from another. In this case, we consider the states for each QD as each of the energy subspaces, so the effective Hamiltonian after the SWT is valid provided that we are far from the resonances (both spin-conserving and spin-flip ones), i.e., $|\delta| \gg \tau_0$, $|\delta \pm E_z| \gg \tau_{\text{sf}}$. Under these conditions, we obtain an effective Hamiltonian that is second order in the tunneling and contains

all contributions due to virtual tunneling to the other dot, given by

$$\hat{H}_{\text{eff}} = \hat{H}_{\text{eff}}^{(0)} + \hat{H}_{\text{eff}}^{(2)}, \quad (31)$$

$$\hat{H}_{\text{eff}}^{(0)} = \frac{\delta}{2} \hat{\tau}_z + \frac{E_z}{2} \hat{\sigma}_z, \quad (32)$$

$$\hat{H}_{\text{eff}}^{(2)} = \frac{\hat{\tau}_z}{2} (-\delta^{(2)} + b_z^{(2)} \hat{\sigma}_z + b_{\perp}^{(2)} \hat{\sigma}_x), \quad (33)$$

where

$$\delta^{(2)} = \frac{2\tau_0^2}{\delta} + \tau_{\text{sf}}^2 \left(\frac{1}{\delta + E_z} + \frac{1}{\delta - E_z} \right), \quad (34a)$$

$$b_z^{(2)} = \tau_{\text{sf}}^2 \left(\frac{1}{\delta + E_z} - \frac{1}{\delta - E_z} \right), \quad (34b)$$

$$b_{\perp}^{(2)} = \tau_0 \tau_{\text{sf}} \left(\frac{1}{\delta + E_z} - \frac{1}{\delta - E_z} \right). \quad (34c)$$

The first term in equation (33) consists of renormalization of the detuning δ due to virtual tunneling. Similarly, the second term is a renormalization of E_z which arises from spin-flip tunneling to the right dot and back. The third term is an effective magnetic field in the direction perpendicular to the external field that gives rise to E_z . It arises from a combination of spin-conserving and spin-flip tunneling. In this process, the spin virtually tunnels to the adjacent dot, flipping its spin, and then tunnels back to the original dot through the spin-conserving path, producing an effective spin rotation. This is the TME discussed in section 2 and, like the OME, arises from the motion of the particle under the SOC (the inter-dot dynamics, in this case). Note that, in the same manner as the OME, the TME requires $E_z \neq 0$ to break the time-reversal symmetry.

The effective magnetic field induced by TME can be used in a similar manner to that of the flopping-mode qubit [65, 67]. However, the qubit cannot be manipulated via detuning alone due to the lack of two-axis control, unless the spin-flip and tunneling amplitudes can be manipulated independently, i.e., unless χ can itself be tuned, e.g., by manipulating the overlap between the particle wave functions centered at each dot [66], rapidly enough to avoid dephasing. Nonetheless, for a time-dependent detuning, as discussed here, the TME allows for resonant manipulation of the dot. Let us focus on the case where $\epsilon_{\text{ac}} \ll \omega$. Then, in the rotating frame and after applying the RWA, we obtain an effective spin model for the resonance $E_z = \omega$. Applying the ac gate with a phase ϕ allows two-axis control of the qubit

$$\hat{H}_{\text{RWA}} = \frac{b_z^{(2)}}{2} \hat{\sigma}_z - \frac{\tilde{b}_{1,\perp}}{2} (\cos \phi \hat{\sigma}_x + \sin \phi \hat{\sigma}_y), \quad (35)$$

where

$$\tilde{b}_{1,\perp} = \frac{4\epsilon_{\text{ac}}\tau_0\tau_{\text{sf}}E_z}{\delta(\delta^2 - E_z^2)}. \quad (36)$$

Otherwise, the frequency of the ac gate can be matched with the renormalized splitting of the two levels of the qubit $E_z + b_z^{(2)}$. The correction to $\tilde{b}_{1,\perp}$ in this case can be given

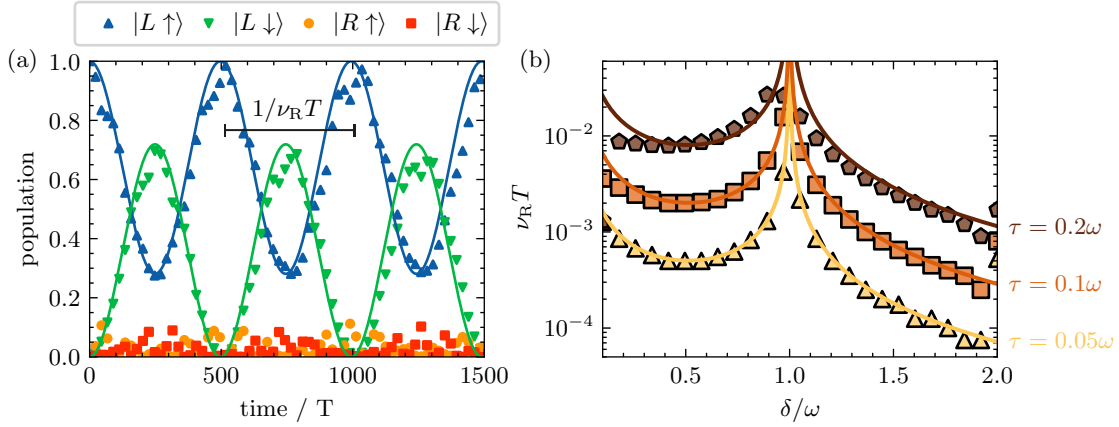


Figure 7. (a) Rabi oscillations in a closed system governed by the full Hamiltonian (symbols) given by equation (2). The dynamics given by the RWA Hamiltonian (solid lines) given by equation (35) is plotted for comparison. Rabi frequency is given by ν_R , shown in the figure. The parameters used are $\delta = \omega/2$ and $\tau = 0.1\omega$. (b) Rabi frequency as a function of detuning for different total tunneling rates. The results are obtained with the full Hamiltonian (symbols) and the effective RWA Hamiltonian (solid lines). The total tunneling rate is $\tau = 0.05\omega$ (yellow, triangles), $\tau = 0.1\omega$ (orange, squares), and $\tau = 0.2\omega$ (brown, pentagons). Other parameters, common for both panels, are $\epsilon_{ac} = 0.2\omega$, $E_z = \omega$, $\chi = 0.2$, and $\beta_{SO} = 0$.

as

$$\tilde{b}_{1,\perp} \rightarrow \tilde{b}_{1,\perp} + \frac{2\epsilon_{ac}\tau_0\tau_{sf}b_z^{(2)}}{(\delta^2 - E_z^2)^2}, \quad (37)$$

which is small in the context of the previous approximations. In figure 7(a), we show the dynamics of the flopping-mode qubit using the effective Hamiltonian described above. For comparison, we also show the result obtained by integrating the equation of motion of a closed system under the original Hamiltonian given by equation (2). Since both dot energy levels are out of resonance, with $\delta = \omega/2$, the population of the right dot is small and the particle remains in the left dot. The results obtained show how the effective model correctly reproduces the dynamics of the system.

The Rabi oscillation frequency of the effective model is given by

$$\nu_R = \frac{1}{2\pi} \sqrt{\left(b_z^{(2)}\right)^2 + \left(\tilde{b}_{1,\perp}\right)^2}. \quad (38)$$

We compare the Rabi frequency of the effective RWA Hamiltonian with that obtained from the original Hamiltonian; see figure 7(b). The results agree for $|\delta - n\omega| \gg \tau$, as expected.

It should be noted that this method of manipulation couples the spin with electric fluctuations due to the dependence of $b_z^{(2)}$ and $b_{\perp}^{(2)}$ on δ . In purified silicon, where the magnetic noise caused by the atomic nuclei is heavily suppressed, this may be the main source of decoherence for the qubit [86, 87]. In the low ac gate amplitude described here, the flopping-mode qubit lacks a natural sweetspot [88, 89] in which the system

is insensitive to electric noise to first order in the coupling to the bath. In particular, electric noise that enters through $b_z^{(2)}$ could only be efficiently suppressed at $\delta = 0$, where the first derivative with respect to δ , i.e., the noise susceptibility, vanishes. However, at this value, the qubit cannot be operated as the direct spin-conserving transition is resonant. However, the perpendicular component of the effective magnetic field of equation (36) can be made insensitive to noise to first order at $\delta = \pm E_z/\sqrt{3}$ which can improve qubit operation. This dynamical sweetspot [57, 90] is observed as a minimum of the Rabi frequency at $\delta \simeq 0.58\omega$ in figure 7(b).

In Appendix B we give expressions for the TME at arbitrary ac detuning amplitudes. Unlike the simple limit shown in equation (36), these expressions are quite complex, highlighting the fact that the effective magnetic field arises from second-order virtual tunneling involving two PAT processes. In the arbitrary-amplitude limit, as given in Appendix B, we can achieve a fine degree of spin manipulation. Furthermore, we also obtain dynamical sweetspots for large ac gate amplitudes.

6. Conclusions

We have studied the effect of SOC on spin transport in a periodically driven DQD. Due to the presence of a spin-flip tunneling path, a highly spin-polarized current can be achieved by tuning the onsite energy difference between the dots. In this direction, we propose several mechanisms to obtain on-demand highly polarized currents in both directions with fully electric control, allowing fast switching of the polarization under experimental conditions. Furthermore, the combination of the orbital dynamics inside the dots and the ac voltage results in the appearance of an effective magnetic field, powering the electric dipole spin resonances in the dots. In transport, the effect of this field can be most clearly observed in the appearance of characteristic avoided crossings of the tunneling resonances near the EDSR condition $E_z \simeq n\omega$. Tunneling under this condition results in striking novel phenomena, such as spin-dependent tunneling amplitudes due to the constructive self-interference of the sidebands coming from the electric and (effective) magnetic fields. Notably, both of these processes arise from the same ac voltage, with the electric field being the direct result of this voltage and the magnetic field effectively incorporating the dynamics of the excited states of the potential. We also investigate the appearance of new dark states when the system is driven under the EDSR condition, resulting from the interference between photo-assisted spin-conserving and spin-flip processes with different numbers of photons involved. Without a Zeeman splitting, time-reversal symmetry protects against destructive interference between these two processes. However, in the presence of a magnetic field, together with an ac voltage, these two paths can interfere and create dark states. These states exhibit a characteristic even-odd effect, appearing only for odd sideband transitions. Moreover, since the current drop is very sharp, its location can be used to characterize the SOC present in the system. These dark states could be useful for quantum information storage, as they are both highly pure and spin-polarized. Finally, we study the viability of flopping-mode qubit operations

when the particle is localized in one of the dots. We provide expressions for the effective magnetic field arising from the interdot motion of the particle under SOC for arbitrary ac-gate amplitudes and particularize the experimentally (more easily) accessible case of small gate amplitudes. In this situation, we identify a dynamical sweetspot induced by the ac voltage, where the Rabi frequency is insensitive to charge noise to first order in detuning. This point of operation may be important for novel solid-state quantum computing platforms, such as isotopically purified silicon, where decoherence due to the nuclear magnetic field can be suppressed, and electric noise may be the most relevant source of decoherence.

Acknowledgments

G.P. and D.F.F. are supported by Spain's MINECO through Grant No. PID2020-117787GB-I00 and by the CSIC Research Platform PTI-001. D.F.F. acknowledges support from FPU Program No. FPU20/04762. J.P.C. acknowledges DFG funding through project B04 of SFB 1277 Emerging Relativistic Phenomena in Condensed Matter. D. F. F. and J. P. C. have contributed equally to this work.

Appendix A. Effective model

In this section, we briefly discuss the origin of the OME term $\hat{H}_1(t)$ in the Hamiltonian of equation (1a). We follow a similar derivation to [69, 91], employing a Schrieffer-Wolff transformation (SWT) to obtain the effective Hamiltonian on the basis employed in the main text. We consider the Hamiltonian for a single particle in a linear DQD (in the x-direction) under both electric and magnetic fields and in the presence of SOC modeled by the spin-orbit vector [92] $\boldsymbol{\alpha} = (\alpha_x, \alpha_y, 0)$ compatible with 2DEGs grown along the [001] direction [93], i.e., the z-direction in our model. We consider an electric field in the x-direction and a Zeeman splitting E_z in the direction normal to the QD plane (in the z-direction). All this together yields the Hamiltonian

$$\hat{H}(x, t) = \hat{H}_k + V(x) + \hat{H}_e(x, t) + \hat{H}_z + \hat{H}_{\text{SO}}, \quad (\text{A.1})$$

$$\hat{H}_k = k^2/2m, \quad (\text{A.2})$$

$$\hat{H}_e(x, t) = exE(t), \quad (\text{A.3})$$

$$\hat{H}_z = E_z \hat{\sigma}_z/2, \quad (\text{A.4})$$

$$\hat{H}_{\text{SO}} = \boldsymbol{\alpha} \cdot \hat{\boldsymbol{\sigma}} k. \quad (\text{A.5})$$

The scalar potential $V(x)$ for the DQD exhibits two minima at $\pm\ell$, near which the potential can be chosen as harmonic $V_{\text{osc}}(x) = (1/2)m\omega_0^2 x^2$. In the tight-binding approximation, we first evaluate the local Hamiltonians in each dot in the eigenfunctions of the individual harmonic potentials

$$|\psi_{\eta, \nu, \sigma}\rangle = |\eta, \nu\rangle|\sigma\rangle, \quad (\text{A.6})$$

with $\nu \in \mathbb{N}$ labeling the eigenstates of the harmonic potential and $\sigma \in \{\uparrow, \downarrow\}$ the spin projection along the z-axis. The orbital part $|\eta, \nu\rangle$ of these eigenfunctions can be

obtained by diagonalizing the Hamiltonian $\hat{H}_k + V_{\text{osc}}(x - \eta\ell)$, with $\eta = \pm$ corresponding to the left and right dots, as appropriate, and corresponds to a Fock-Darwin function with shifted centers. Following this, around $\eta\ell$ we can write the terms of the Hamiltonian as

$$\hat{H}_k + V_{\text{osc}}(x - \eta\ell) = \omega_0 (\hat{a}^\dagger \hat{a} + 1), \quad (\text{A.7})$$

$$\hat{H}_e(\eta\ell, t) = el_0 E(t) (\hat{a}^\dagger + \hat{a}) + e\eta E(t) \ell, \quad (\text{A.8})$$

$$\hat{H}_{\text{SO}} = \frac{i}{2l_0} \boldsymbol{\alpha} \cdot \hat{\boldsymbol{\sigma}} (\hat{a}^\dagger - \hat{a}), \quad (\text{A.9})$$

with \hat{a}^\dagger, \hat{a} the Fock operators of the oscillator and the Zeeman term unchanged. Moreover, we employ the characteristic oscillator length $l_0 = \sqrt{\omega_0/2m}$. We can separate this Hamiltonian into a part that is static in the orbital dynamics

$$\hat{H}_\eta^{(0)} = \omega_0 (\hat{a}^\dagger \hat{a} + 1) + eE(t) \eta\ell + (E_z/2) \hat{\sigma}_z, \quad (\text{A.10})$$

and a dynamic part

$$\hat{H}_\eta^{(1)} = el_0 E(t) (\hat{a}^\dagger + \hat{a}) + (i/2l_0) \boldsymbol{\alpha} \cdot \hat{\boldsymbol{\sigma}} (\hat{a}^\dagger - \hat{a}). \quad (\text{A.11})$$

When projected into the ground state, the first part reduces to the usual description of single-state QDs. However, if we project the second part as well, we will obtain an effective Hamiltonian that incorporates the action of the SOC into the ground state. We do this by first performing a SWT $\hat{H}'_\eta(t) = e^{\hat{\Upsilon}} \hat{H}_\eta(t) e^{-\hat{\Upsilon}}$. We further consider the adiabatic approximation with respect to the electric field, valid provided that the driving frequency is much lower than the oscillator frequency, i.e., $\omega \ll \omega_0$. Then the anti-Hermitian operator $\hat{\Upsilon}$ is given by

$$[\hat{H}_\eta^{(0)}, \hat{\Upsilon}] = \hat{H}_\eta^{(1)}, \quad (\text{A.12})$$

resulting in

$$\hat{\Upsilon} = (f + \mathbf{d} \cdot \hat{\boldsymbol{\sigma}}) \hat{a}^\dagger - (f^* + \mathbf{d}^* \cdot \hat{\boldsymbol{\sigma}}) \hat{a}, \quad (\text{A.13})$$

where

$$f = el_0 E_\eta(t) / \omega_0, \quad (\text{A.14})$$

$$d_x = \frac{1}{2l_0} \frac{i\omega_0 \alpha_x + \alpha_y E_z}{\omega_0^2 - E_z^2}, \quad (\text{A.15})$$

$$d_y = \frac{1}{2l_0} \frac{i\omega_0 \alpha_y - \alpha_x E_z}{\omega_0^2 - E_z^2}, \quad (\text{A.16})$$

$$d_z = 0. \quad (\text{A.17})$$

The effective action of the SOC term in the ground state is described by the Hamiltonian

$$\begin{aligned} \hat{H}_\eta^{(2)} = \frac{1}{2} [\hat{\Upsilon}, \hat{H}_\eta^{(1)}] = \frac{1}{2} \{ & [(f + \mathbf{d} \cdot \hat{\boldsymbol{\sigma}}), (el_0 E(t) + (i/2l_0) \boldsymbol{\alpha} \cdot \hat{\boldsymbol{\sigma}})] \hat{a}^\dagger \hat{a}^\dagger \\ & - [(f^* + \mathbf{d}^* \cdot \hat{\boldsymbol{\sigma}}), (el_0 E(t) - (i/2l_0) \boldsymbol{\alpha} \cdot \hat{\boldsymbol{\sigma}})] \hat{a} \hat{a} \\ & + [(f + \mathbf{d} \cdot \hat{\boldsymbol{\sigma}}), (el_0 E(t) - (i/2l_0) \boldsymbol{\alpha} \cdot \hat{\boldsymbol{\sigma}})] \hat{a}^\dagger \hat{a} \\ & + (el_0 E(t) - (i/2l_0) \boldsymbol{\alpha} \cdot \hat{\boldsymbol{\sigma}}) (f + \mathbf{d} \cdot \hat{\boldsymbol{\sigma}}) \\ & + [(el_0 E(t) + (i/2l_0) \boldsymbol{\alpha} \cdot \hat{\boldsymbol{\sigma}}), (f^* + \mathbf{d}^* \cdot \hat{\boldsymbol{\sigma}})] \hat{a}^\dagger \hat{a} \\ & + (f^* + \mathbf{d}^* \cdot \hat{\boldsymbol{\sigma}}) (el_0 E(t) + (i/2l_0) \boldsymbol{\alpha} \cdot \hat{\boldsymbol{\sigma}}) \}. \end{aligned} \quad (\text{A.18})$$

The two-pair excitation processes ($\propto \hat{a}\hat{a}, \hat{a}^\dagger\hat{a}^\dagger$) connect states that are separated in energy by $2\omega_0$ and therefore can be neglected in our effective Hamiltonian approximation, while the terms $\propto \hat{a}^\dagger\hat{a}$ do not contribute to the energy of the ground state. Hence, we find the following

$$\hat{H}_\eta^{(2)} = \frac{-E_z||\boldsymbol{\alpha}||^2}{2l_0^2(\omega_0^2 - E_z^2)}\hat{\sigma}_z + \frac{E_z e E(t)}{\omega_0^2 - E_z^2}\boldsymbol{\alpha}^\perp \cdot \hat{\boldsymbol{\sigma}}. \quad (\text{A.19})$$

where $\boldsymbol{\alpha}^\perp = (\alpha_y, -\alpha_x, 0)$. The first term shifts the Zeeman splitting to

$$\tilde{E}_z = E_z \left(1 - \frac{||\boldsymbol{\alpha}||^2}{2l_0^2(\omega_0^2 - E_z^2)} \right), \quad (\text{A.20})$$

while the second term is the OME field that we sought. Crucially, it is oriented perpendicular to the direction of the SOC field, i.e., to $\boldsymbol{\alpha}$. Note that both terms require $E_z \neq 0$ to break the time-reversal symmetry. Moreover, the constant part of the electric field $E(t)$ in the second term will rotate the spin quantization axis. However, this rotation is produced around the direction determined by $\boldsymbol{\alpha}$. As shown in the following, the spin-flip amplitude is aligned in this direction and is unaffected by this rotation. The Zeeman splitting along the new quantization axis is given by

$$\tilde{E}_z \rightarrow \tilde{E}_z \sqrt{1 + \frac{e^2 E_0^2 ||\boldsymbol{\alpha}||^4}{(\omega_0^2 - E_z^2)^2}} \approx \tilde{E}_z \left(1 + \frac{e^2 E_0^2 ||\boldsymbol{\alpha}||^4}{2(\omega_0^2 - E_z^2)^2} \right), \quad (\text{A.21})$$

with E_0 being the constant part of the electric field. This is a next-order effect compared to the shift from E_z to \tilde{E}_z and can be ignored. The OME term is similarly rotated, but this is also a higher-order effect, and we disregard it as well.

Regarding tunneling amplitudes, we consider orthonormal Wannier functions of the ground state of each dot, defined as [66]

$$|w_{\eta,\sigma}\rangle = \frac{1}{\sqrt{N}}(|\psi_{\eta,0,\sigma}\rangle + \gamma|\psi_{\bar{\eta},0,\sigma}\rangle), \quad (\text{A.22})$$

where $N \equiv 1 - 2\gamma S + \gamma^2$, $\gamma \equiv (1 - \sqrt{1 - S^2})/S$, and $S \equiv \langle \psi_{L,0,\sigma} | \psi_{R,0,\sigma} \rangle$ is the overlap between the dot wave functions. Regardless of the particularities of $V(x)$, we can consider a standard real-valued tunneling matrix element τ_0 without loss of generality. The spin-flip tunneling amplitude can be obtained as

$$\tau_{\text{sf}} = \langle w_{L\sigma} | \hat{H}_{\text{SO}} | w_{R\sigma'} \rangle = \frac{1 - \gamma^2}{N} \langle \sigma | \boldsymbol{\alpha} \cdot \hat{\boldsymbol{\sigma}} | \sigma' \rangle \langle L, 0 | k | R, 0 \rangle, \quad (\text{A.23})$$

with $|\eta, 0\rangle$ the ground state of the respective harmonic oscillator, as defined above. The general form of the expected value $\langle L, 0 | k | R, 0 \rangle$ can be determined by imposing time-reversal invariance of the spin-orbit Hamiltonian, i.e., $\mathcal{T} \hat{H}_{\text{SO}} \mathcal{T}^{-1} = \hat{H}_{\text{SO}}$. In the most general way, the SOC Hamiltonian, written on the basis of $\{|L \uparrow\rangle, |L \downarrow\rangle, |R \uparrow\rangle, |R \downarrow\rangle\}$, reads as follows

$$\hat{H}_{\text{SO}} = \begin{pmatrix} 0 & 0 & 0 & \tau_{\text{sf}} \\ 0 & 0 & -\tau_{\text{sf}}^* & 0 \\ 0 & -\tau_{\text{sf}} & 0 & 0 \\ \tau_{\text{sf}}^* & 0 & 0 & 0 \end{pmatrix}. \quad (\text{A.24})$$

Taking α along the y-direction, as considered throughout this work, we recover a term $\propto \hat{\tau}_y \hat{\sigma}_y$, which yields a real spin-flip matrix of the form

$$\hat{H}_{\text{SO}} = \begin{pmatrix} 0 & 0 & 0 & \tau_{\text{sf}} \\ 0 & 0 & -\tau_{\text{sf}} & 0 \\ 0 & -\tau_{\text{sf}} & 0 & 0 \\ \tau_{\text{sf}} & 0 & 0 & 0 \end{pmatrix}. \quad (\text{A.25})$$

The fact that the spin-flip tunneling term is $\propto \hat{\tau}_y$ is crucial. Otherwise, the spin-flip and spin-conserving tunneling terms can interfere destructively. Consider, for instance, that the tunneling is of the form $\propto \hat{\tau}_x \hat{\sigma}_x$. By performing a $\pi/2$ rotation around the y-axis, we obtain

$$\hat{H}_{\text{T}} = \begin{pmatrix} 0 & 0 & -\tau_0 + \tau_{\text{sf}} & 0 \\ 0 & 0 & 0 & -\tau_0 - \tau_{\text{sf}} \\ -\tau_0 + \tau_{\text{sf}} & 0 & 0 & 0 \\ 0 & -\tau_0 - \tau_{\text{sf}} & 0 & 0 \end{pmatrix}, \quad (\text{A.26})$$

which can exhibit a dark state when $\tau_0 = \tau_{\text{sf}}$, i.e., when $\chi = 0.5$. However, if, as here, we have a term $\propto \hat{\tau}_y \hat{\sigma}_y$, the rotation yields

$$\hat{H}_{\text{T}} = \begin{pmatrix} 0 & 0 & -\tau_0 - i\tau_{\text{sf}} & 0 \\ 0 & 0 & 0 & -\tau_0 + i\tau_{\text{sf}} \\ -\tau_0 + i\tau_{\text{sf}} & 0 & 0 & 0 \\ 0 & -\tau_0 - i\tau_{\text{sf}} & 0 & 0 \end{pmatrix}, \quad (\text{A.27})$$

preventing destructive interference.

Appendix B. TME for arbitrary ac amplitudes

In this appendix, we give the expressions for the TME terms in the time-dependent case with arbitrary ac amplitudes. After a time-dependent SWT [94], we obtain an effective Hamiltonian up to second order in the tunnel couplings, given by

$$\hat{H}_{\text{eff}}^{(2)}(t) = \frac{\hat{\tau}_z}{2} \{ -\delta^{(2)}(t) + b_z^{(2)}(t) \hat{\sigma}_z + [b_x^{(2)}(t) \hat{\sigma}_x + b_y^{(2)}(t) \hat{\sigma}_y] \}, \quad (\text{B.1})$$

where the time-dependent detuning and Zeeman splittings are given by

$$\begin{aligned} \delta^{(2)}(t) &= \sum_{\mu, \nu} J_{\mu} \left(\frac{\epsilon_{\text{ac}}}{\omega} \right) J_{\nu} \left(\frac{\epsilon_{\text{ac}}}{\omega} \right) \cos[(\mu - \nu)\omega t] \\ &\quad \times \left[\frac{2\tau_0^2}{\delta - \nu\omega} + \frac{\tau_{\text{sf}}^2}{\delta + E_z + \nu\omega} + \frac{\tau_{\text{sf}}^2}{\delta - E_z + \nu\omega} \right], \end{aligned} \quad (\text{B.2})$$

$$\begin{aligned} b_z^{(2)}(t) &= \sum_{\mu, \nu} J_{\mu} \left(\frac{\epsilon_{\text{ac}}}{\omega} \right) J_{\nu} \left(\frac{\epsilon_{\text{ac}}}{\omega} \right) \cos[(\mu - \nu)\omega t] \\ &\quad \times \left[\frac{\tau_{\text{sf}}^2}{\delta + E_z + \nu\omega} - \frac{\tau_{\text{sf}}^2}{\delta - E_z + \nu\omega} \right]. \end{aligned} \quad (\text{B.3})$$

The magnetic field gradient in the perpendicular direction is given by

$$b_x^{(2)}(t) = \sum_{\mu,\nu} J_\mu \left(\frac{\epsilon_{ac}}{\omega} \right) J_\nu \left(\frac{\epsilon_{ac}}{\omega} \right) \cos[(\mu - \nu)(\omega t + \phi)] \\ \times \left[\frac{\tau_0 \tau_{sf}}{\delta + E_z - \nu\omega} - \frac{\tau_0 \tau_{sf}}{\delta - E_z - \nu\omega} \right] \quad (B.4)$$

$$b_y^{(2)}(t) = \sum_{\mu,\nu} J_\mu \left(\frac{\epsilon_{ac}}{\omega} \right) J_\nu \left(\frac{\epsilon_{ac}}{\omega} \right) \sin[(\mu - \nu)(\omega t + \phi)] \\ \times \left(\frac{2\tau_0 \tau_{sf}}{\delta - \nu\omega} - \frac{\tau_0 \tau_{sf}}{\delta + E_z - \nu\omega} - \frac{\tau_0 \tau_{sf}}{\delta - E_z - \nu\omega} \right). \quad (B.5)$$

Note that these expressions involve two different photon numbers μ and ν , as they are virtual second-order tunneling processes that involve two photo-assisted transitions [55, 57].

In an n -photon resonance $E_z \simeq n\omega$, the Hamiltonian in the RWA is given by

$$\hat{H}_n^{(2)}(t) = \frac{\hat{\tau}_z}{2} \{ -\tilde{\delta}^{(2)} + (E_z + \tilde{b}_z^{(2)} - n\omega) \hat{\sigma}_z + \tilde{b}_{n,\perp}^{(2)} [\cos(n\phi) \hat{\sigma}_x + \sin(n\phi) \hat{\sigma}_y] \}, \quad (B.6)$$

where the diagonal terms are given by

$$\tilde{\delta}^{(2)} = \sum_\nu J_\nu^2 \left(\frac{\epsilon_{ac}}{\omega} \right) \left[\frac{2\tau_0^2}{\delta - \nu\omega} + \frac{\tau_{sf}^2}{\delta + E_z + \nu\omega} + \frac{\tau_{sf}^2}{\delta - E_z + \nu\omega} \right], \quad (B.7)$$

$$\tilde{b}_z^{(2)} = \sum_\nu J_\nu^2 \left(\frac{\epsilon_{ac}}{\omega} \right) \left(\frac{\tau_{sf}^2}{\delta + E_z + \nu\omega} - \frac{\tau_{sf}^2}{\delta - E_z + \nu\omega} \right), \quad (B.8)$$

and the off-diagonal term has an amplitude

$$\tilde{b}_{n,\perp}^{(2)} = \sum_\nu J_\nu \left(\frac{\epsilon_{ac}}{\omega} \right) J_{\nu+n} \left(\frac{\epsilon_{ac}}{\omega} \right) \left(\frac{\tau_0 \tau_{sf}}{\delta - \nu\omega} - \frac{\tau_0 \tau_{sf}}{\delta - E_z - \nu\omega} \right) \\ - \sum_\nu J_\nu \left(\frac{\epsilon_{ac}}{\omega} \right) J_{\nu-n} \left(\frac{\epsilon_{ac}}{\omega} \right) \left(\frac{\tau_0 \tau_{sf}}{\delta - \nu\omega} - \frac{\tau_0 \tau_{sf}}{\delta + E_z - \nu\omega} \right). \quad (B.9)$$

If figure B1, we compare the Rabi frequency of a flopping-mode qubit obtained with the full Hamiltonian, with the results given by the effective RWA Hamiltonian shown above. To obtain numerical results, we have truncated the summations to $\nu = -2, -1, \dots, 2$. The agreement between both results is notable, even when working with tunneling rates of $\tau = 0.2\omega$. We also compare the prediction given by the low-amplitude effective Hamiltonian shown in equation (35) of the main text. In the limit of $\epsilon_{ac} < \omega/2$ all the results coincide.

Appendix C. TME under the spin resonance condition: asymmetry in δ

To gain insight into the asymmetry in δ discussed in section 3.1 of the main text, let us study the TME under spin resonance. That is, we consider the Hamiltonian of equation (24) in a situation where direct tunneling between the two dots is energetically disfavored. This can always be satisfied by lowering τ . Hence, since in this appendix we are concerned with qualitative understanding of the asymmetry, we do not regard the

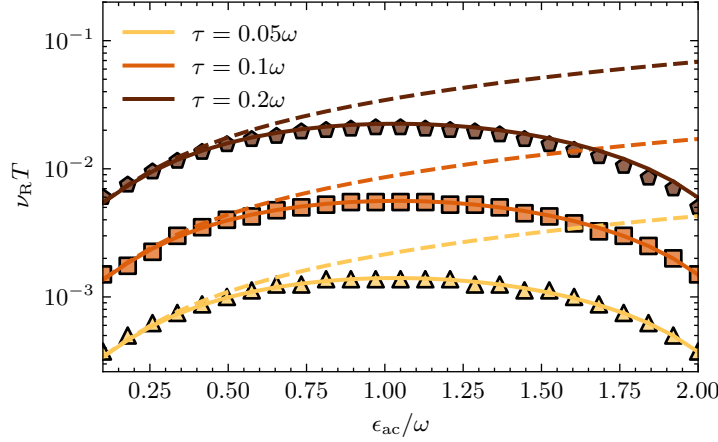


Figure B1. Rabi frequency as a function of driving amplitude for different total tunneling rates. The results are obtained with the full Hamiltonian (symbols), the low-amplitude effective RWA Hamiltonian (dashed lines) shown in equation (35) of the main text, and the RWA Hamiltonian (solid lines) of equation (B.6) taking into account up to five terms in the infinite series. The total tunneling rate is $\tau = 0.05\omega$ (yellow, triangles), $\tau = 0.1\omega$ (orange, squares), and $\tau = 0.2\omega$ (brown, pentagons). Other parameters are $E_z = \omega$, $\delta = \omega/2$, $\chi = 0.2$ and $\beta_{\text{SO}} = 0$.

precise conditions of validity and always assume a value of τ that makes the SWT valid. Under this condition, virtual tunneling processes are dominant and we can employ a SWT to obtain an effective Hamiltonian with the leading term being of second order in the tunneling amplitudes, as done above for the flopping-mode operation in section 5 of the main text. We apply these transformations in the frame discussed in section 3.1 leading to equation (24), i.e., after applying equation (16) and equation (13)), and working in the RWA. This is different from the treatment of Appendix B, where SWT was applied before RWA. This amounts to neglecting photo-assisted virtual tunneling processes. A complete treatment of the TME in the presence of the OME lies outside of the scope of this work.

In this rotating frame, as discussed above, the β_{SO} term has taken a role analogous to the Zeeman splitting. Applying the transformation yields the following effective spin model for the left dot

$$\hat{H}_{\text{eff}} = \frac{1}{2} \left(\tilde{E}_z + \tilde{b}_z^{(2)} \right) \hat{\sigma}_z + \frac{\tilde{b}_\perp^{(2)}}{2} \hat{\sigma}_x, \quad (\text{C.1})$$

where the effective magnetic field is given by

$$\tilde{b}_z^{(2)} = \frac{\tilde{\tau}_\downarrow^2 - \tilde{\tau}_\uparrow^2}{\delta} + \frac{2\tilde{E}_z \tilde{\tau}_{\text{sf}}^2}{\tilde{E}_z^2 - \delta^2}, \quad (\text{C.2})$$

$$\tilde{b}_\perp^{(2)} = \tilde{\tau}_{\text{sf}} \left(\frac{\tilde{\tau}_\downarrow}{\tilde{E}_z - \delta} - \frac{\tilde{\tau}_\uparrow}{\tilde{E}_z + \delta} - \frac{\tilde{\tau}_\uparrow + \tilde{\tau}_\downarrow}{\delta} \right). \quad (\text{C.3})$$

The term $\tilde{b}_z^{(2)}$ is non-zero in the presence of spin-dependent tunneling amplitudes $|\tilde{\tau}_\uparrow| \neq |\tilde{\tau}_\downarrow|$, and a finite spin-flip tunneling rate $\tilde{\tau}_{\text{sf}}$. The effective Hamiltonian is not

symmetric (nor antisymmetric) in δ . However, it is symmetric under reflection $\delta \rightarrow -\delta$ and $\epsilon_{ac} \rightarrow -\epsilon_{ac}$. Under this reflection, the effective tunneling rates transform as $\tilde{\tau}_{\uparrow} \rightleftharpoons \tilde{\tau}_{\downarrow}$, and $\tilde{\tau}_{sf} \rightarrow -\tilde{\tau}_{sf}$ for an odd resonance $E_z = (2k + 1)\omega$, $k \in \mathbb{Z}$, as discussed in section 3.1.

References

- [1] Pribiag V S, Nadj-Perge S, Frolov S M, van den Berg J W G, van Weperen I, Plissard S R, Bakkers E P A M and Kouwenhoven L P 2013 *Nature Nanotechnology* **8** 170–174
- [2] Bogan A, Studenikin S, Korkusinski M, Aers G, Gaudreau L, Zawadzki P, Sachrajda A, Tracy L, Reno J and Hargett T 2017 *Physical Review Letters* **118** 167701
- [3] Vukušić L, Kukučka J, Watzinger H, Milem J M, Schäffler F and Katsaros G 2018 *Nano Letters* **18** 7141–7145
- [4] Hendrickx N W, Franke D P, Sammak A, Scappucci G and Veldhorst M 2020 *Nature* **577** 487–491
- [5] van Riggelen F, Hendrickx N W, Lawrie W I L, Russ M, Sammak A, Scappucci G and Veldhorst M 2021 *Applied Physics Letters* **118** 044002
- [6] Froning F N M, Rančić M J, Hetényi B, Bosco S, Rehmann M K, Li A, Bakkers E P A M, Zwanenburg F A, Loss D, Zumbühl D M and Braakman F R 2021 *Physical Review Research* **3** 013081
- [7] Hendrickx N W, Lawrie W I L, Russ M, van Riggelen F, de Snoo S L, Schouten R N, Sammak A, Scappucci G and Veldhorst M 2021 *Nature* **591** 580–585
- [8] van Riggelen F, Lawrie W I L, Russ M, Hendrickx N W, Sammak A, Rispler M, Terhal B M, Scappucci G and Veldhorst M 2022 *npj Quantum Information* **8**
- [9] Kloeffer C and Loss D 2013 *Annual Review of Condensed Matter Physics* **4** 51–81
- [10] Veldhorst M, Eenink H G J, Yang C H and Dzurak A S 2017 *Nature Communications* **8**
- [11] Zhang X, Li H O, Cao G, Xiao M, Guo G C and Guo G P 2018 *National Science Review* **6** 32–54
- [12] Kandel Y P, Qiao H, Fallahi S, Gardner G C, Manfra M J and Nichol J M 2019 *Nature* **573** 553–557
- [13] Scappucci G, Kloeffer C, Zwanenburg F A, Loss D, Myronov M, Zhang J J, Franceschi S D, Katsaros G and Veldhorst M 2020 *Nature Reviews Materials* **6** 926–943
- [14] Langrock, Veit and Krzywda, Jan A and Focke, Niels and Seidler, Inga and Schreiber, Lars R and Cywiński, Lukasz 2022 Blueprint of a scalable spin qubit shuttle device for coherent mid-range qubit transfer in disordered Si/SiGe/SiO₂ URL <https://arxiv.org/abs/2202.11793>
- [15] Koppens F H L, Buizert C, Tielrooij K J, Vink I T, Nowack K C, Meunier T, Kouwenhoven L P and Vandersypen L M K 2006 *Nature* **442** 766–771
- [16] Nowack K C, Koppens F H L, Nazarov Y V and Vandersypen L M K 2007 *Science* **318** 1430–1433
- [17] Veldhorst M, Yang C H, Hwang J C C, Huang W, Dehollain J P, Muhonen J T, Simmons S, Laucht A, Hudson F E, Itoh K M, Morello A and Dzurak A S 2015 *Nature* **526** 410–414
- [18] Zwerver A M J, Krähenmann T, Watson T F, Lampert L, George H C, Pillarisetty R, Bojarski S A, Amin P, Amitonov S V, Boter J M, Caudillo R, Correias-Serrano D, Dehollain J P, Droulers G, Henry E M, Kotlyar R, Lodari M, Lüthi F, Michalak D J, Mueller B K, Neyens S, Roberts J, Samkharadze N, Zheng G, Zietz O K, Scappucci G, Veldhorst M, Vandersypen L M K and Clarke J S 2022 *Nature Electronics* **5** 184–190
- [19] Szumniak P, Bednarek S, Partoens B and Peeters F M 2012 *Physical Review Letters* **109** 107201
- [20] Watzinger H, Kukučka J, Vukušić L, Gao F, Wang T, Schäffler F, Zhang J J and Katsaros G 2018 *Nature Communications* **9**
- [21] Hendrickx N W, Lawrie W I L, Petit L, Sammak A, Scappucci G and Veldhorst M 2020 *Nature Communications* **11**
- [22] Jirovec D, Hofmann A, Ballabio A, Mutter P M, Tavani G, Botifoll M, Crippa A, Kukučka J, Sagi O, Martins F, Saez-Mollejo J, Prieto I, Borovkov M, Arbiol J, Chrastina D, Isella G and Katsaros G 2021 *Nature Materials* **20** 1106–1112

- [23] Mutter P M and Burkard G 2021 *Physical Review B* **104** 195421
- [24] Bosco S, Benito M, Adelsberger C and Loss D 2021 *Physical Review B* **104** 115425
- [25] Froning F N M, Camenzind L C, van der Molen O A H, Li A, Bakkers E P A M, Zumbühl D M and Braakman F R 2021 *Nature Nanotechnology* **16** 308–312
- [26] Bosco S and Loss D 2021 *Physical Review Letters* **127** 190501
- [27] Bosco S, Hetényi B and Loss D 2021 *PRX Quantum* **2** 010348
- [28] Jirovec D, Mutter P M, Hofmann A, Crippa A, Rychetsky M, Craig D L, Kukucka J, Martins F, Ballabio A, Ares N, Chrastina D, Isella G, Burkard G and Katsaros G 2022 *Physical Review Letters* **128** 126803
- [29] Wang K, Xu G, Gao F, Liu H, Ma R L, Zhang X, Wang Z, Cao G, Wang T, Zhang J J, Culcer D, Hu X, Jiang H W, Li H O, Guo G C and Guo G P 2022 *Nature Communications* **13**
- [30] Fernández-Fernández D, Ban Y and Platero G 2022 *Physical Review Applied* **18** 054090
- [31] Tokura Y, van der Wiel W G, Obata T and Tarucha S 2006 *Physical Review Letters* **96** 047202
- [32] Pioro-Ladrière M, Obata T, Tokura Y, Shin Y S, Kubo T, Yoshida K, Taniyama T and Tarucha S 2008 *Nature Physics* **4** 776–779
- [33] Watson T F, Philips S G J, Kawakami E, Ward D R, Scarlino P, Veldhorst M, Savage D E, Lagally M G, Friesen M, Coppersmith S N, Eriksson M A and Vandersypen L M K 2018 *Nature* **555** 633–637
- [34] Laird E A, Barthel C, Rashba E I, Marcus C M, Hanson M P and Gossard A C 2007 *Physical Review Letters* **99** 246601
- [35] Ribeiro H, Petta J R and Burkard G 2010 *Physical Review B* **82** 115445
- [36] Crippa A, Maurand R, Bourdet L, Kotekar-Patil D, Amissé A, Jehl X, Sanquer M, Laviéville R, Bohuslavskiy H, Hutin L, Barraud S, Vinet M, Niquet Y M and Franceschi S D 2018 *Physical Review Letters* **120** 137702
- [37] Hofmann A, Jirovec D, Borovkov M, Prieto I, Ballabio A, Frigerio J, Chrastina D, Isella G and Katsaros G 2019 ‘Assessing the potential of Ge/SiGe quantum dots as hosts for singlet-triplet qubits (*Preprint* [1910.05841](https://arxiv.org/abs/1910.05841))
- [38] Liles S D, Martins F, Miserev D S, Kiselev A A, Thorvaldson I D, Rendell M J, Jin I K, Hudson F E, Veldhorst M, Itoh K M, Sushkov O P, Ladd T D, Dzurak A S and Hamilton A R 2021 *Physical Review B* **104** 235303
- [39] Zajac D M, Sigillito A J, Russ M, Borjans F, Taylor J M, Burkard G and Petta J R 2018 *Science* **359** 439–442
- [40] Liu Z H, Li R, Hu X and You J Q 2018 *Scientific Reports* **8**
- [41] Burkard G, Ladd T D, Nichol J M, Pan A and Petta J R 2021 Semiconductor Spin Qubits URL <https://arxiv.org/abs/2112.08863>
- [42] Noiri A, Takeda K, Nakajima T, Kobayashi T, Sammak A, Scappucci G and Tarucha S 2022 *Nature* **601** 338–342
- [43] Vahapoglu E, Slack-Smith J P, Leon R C C, Lim W H, Hudson F E, Day T, Cifuentes J D, Tanttu T, Yang C H, Saraiva A, Abrosimov N V, Pohl H J, Thewalt M L W, Laucht A, Dzurak A S and Pla J J 2022 *npj Quantum Information* **8**
- [44] Philips S G J, Madzik M T, Amitonov S V, de Snoo S L, Russ M, Kalhor N, Volk C, Lawrie W I L, Brousse D, Tryputen L, Wuetz B P, Sammak A, Veldhorst M, Scappucci G and Vandersypen L M K 2022 *Nature* **609** 919–924
- [45] Takeda K, Noiri A, Nakajima T, Kobayashi T and Tarucha S 2022 *Nature* **608** 682–686
- [46] Mills A R, Guinn C R, Gullans M J, Sigillito A J, Feldman M M, Nielsen E and Petta J R 2022 *Science Advances* **8**
- [47] Xue X, Russ M, Samkharadze N, Undseth B, Sammak A, Scappucci G and Vandersypen L M K 2022 *Nature* **601** 343–347
- [48] Dunlap D H and Kenkre V M 1986 *Physical Review B* **34** 3625–3633
- [49] Grossmann F, Dittrich T, Jung P and Hänggi P 1991 *Phys. Rev. Lett.* **67**(4) 516–519 URL <https://link.aps.org/doi/10.1103/PhysRevLett.67.516>

- [50] Barata J C A and Wreszinski W F 2000 *Physical Review Letters* **84** 2112–2115
- [51] Gómez-León A and Platero G 2011 *Phys. Rev. B* **84**(12) 121310 URL <https://link.aps.org/doi/10.1103/PhysRevB.84.121310>
- [52] Hanson R, Vandersypen L M K, van Beveren L H W, Elzerman J M, Vink I T and Kouwenhoven L P 2004 *Physical Review B* **70** 241304
- [53] Cota E, Aguado R and Platero G 2005 *Physical Review Letters* **94** 107202
- [54] Sánchez R, Cota E, Aguado R and Platero G 2006 *Physica E: Low-dimensional Systems and Nanostructures* **34** 405–408
- [55] Gallego-Marcos F, Sánchez R and Platero G 2015 *Journal of Applied Physics* **117** 112808
- [56] Stano P, Klinovaja J, Braakman F R, Vandersypen L M K and Loss D 2015 *Physical Review B* **92** 075302
- [57] Picó-Cortés J, Gallego-Marcos F and Platero G 2019 *Physical Review B* **99** 155421
- [58] Grifoni M and Hänggi P 1998 *Physics Reports* **304** 229–354
- [59] Platero G and Aguado R 2004 *Physics Reports* **395** 1–157
- [60] Eckardt A and Anisimovas E 2015 *New Journal of Physics* **17** 093039 URL <https://doi.org/10.1088/1367-2630/17/9/093039>
- [61] Sala A and Danon J 2021 *Physical Review B* **104** 085421
- [62] Zhou Y, Gu S, Wang K, Cao G, Hu X, Gong M, Guo G C, Li H O and Guo G P 2021 Full tunability enabled by Floquet engineering in a multilevel quantum dot system URL <https://arxiv.org/abs/2110.09852>
- [63] Zhou Y, Wang K, Liu H, Cao G, Guo G C, Hu X, Li H O and Guo G P 2022 Quantum Interference and Coherent Population Trapping in a Double Quantum Dot URL <https://arxiv.org/abs/2209.14528>
- [64] Khomitsky D V and Studenikin S A 2022 *Physical Review B* **106** 195414
- [65] Croot X, Mi X, Putz S, Benito M, Borjans F, Burkard G and Petta J R 2020 *Physical Review Research* **2** 012006
- [66] Mütter P M and Burkard G 2021 *Physical Review Research* **3** 013194
- [67] Teske J D, Butt F, Cerfontaine P, Burkard G and Bluhm H 2023 *Physical Review B* **107** 035302
- [68] Burkard G and Loss D 2002 *Phys. Rev. Lett.* **88**(4) 047903 URL <https://link.aps.org/doi/10.1103/PhysRevLett.88.047903>
- [69] Rashba E I 2008 *Phys. Rev. B* **78**(19) 195302 URL <https://link.aps.org/doi/10.1103/PhysRevB.78.195302>
- [70] Khomitsky D and Sherman E 2011 *Nanoscale Research Letters* **6** URL <https://doi.org/10.1186/1556-276x-6-212>
- [71] Maisi V F, Hofmann A, Rösli M, Basset J, Reichl C, Wegscheider W, Ihn T and Ensslin K 2016 *Phys. Rev. Lett.* **116**(13) 136803 URL <https://link.aps.org/doi/10.1103/PhysRevLett.116.136803>
- [72] Bogan A, Studenikin S, Korkusinski M, Gaudreau L, Zawadzki P, Sachrajda A S, Tracy L, Reno J and Hargett T 2018 *Physical Review Letters* **120** 207701
- [73] Bogan A, Studenikin S, Korkusinski M, Gaudreau L, Phoenix J, Zawadzki P, Sachrajda A, Tracy L, Reno J and Hargett T 2021 *Phys. Rev. B* **103**(23) 235310 URL <https://link.aps.org/doi/10.1103/PhysRevB.103.235310>
- [74] Rohrmeier C and Donarini A 2021 *Phys. Rev. B* **103**(20) 205420 URL <https://link.aps.org/doi/10.1103/PhysRevB.103.205420>
- [75] Kohler S, Lehmann J and Hänggi P 2005 *Physics Reports* **406** 379–443 ISSN 0370-1573 URL <https://www.sciencedirect.com/science/article/pii/S0370157304005071>
- [76] Gurvitz S A and Prager Y S 1996 *Physical Review B* **53** 15932–15943
- [77] Michaelis B, Emary C and Beenakker C W J 2006 *Europhysics Letters* **73** 677 URL <https://dx.doi.org/10.1209/epl/i2005-10458-6>
- [78] Pörtl C, Emary C and Brandes T 2009 *Phys. Rev. B* **80**(11) 115313 URL <https://link.aps.org/doi/10.1103/PhysRevB.80.115313>

- [79] Busl M, Sánchez R and Platero G 2010 *Phys. Rev. B* **81**(12) 121306 URL <https://link.aps.org/doi/10.1103/PhysRevB.81.121306>
- [80] Donarini A, Niklas M, Schaffberger M, Paradiso N, Strunk C and Grifoni M 2019 *Nature Communications* **10** URL <https://doi.org/10.1038/s41467-018-08112-x>
- [81] Villavicencio J, Maldonado I, Cota E and Platero G 2011 *New Journal of Physics* **13** 023032
- [82] Stehlik J, Schroer M, Maialle M, Degani M and Petta J 2014 *Physical Review Letters* **112** 227601
- [83] Danon J and Rudner M S 2014 *Physical Review Letters* **113** 247002
- [84] Demkov Y N and Kurasov P B 2007 *Theoretical and Mathematical Physics* **153** 1407–1422
- [85] Creffield C 2003 *Physical Review B* **67** 165301
- [86] Tyryshkin A M, Tojo S, Morton J J L, Riemann H, Abrosimov N V, Becker P, Pohl H J, Schenkel T, Thewalt M L W, Itoh K M and Lyon S A 2011 *Nature Materials* **11** 143–147 URL <https://doi.org/10.1038/nmat3182>
- [87] Veldhorst M, Hwang J C C, Yang C H, Leenstra A W, de Ronde B, Dehollain J P, Muhonen J T, Hudson F E, Itoh K M, Morello A and Dzurak A S 2014 *Nature Nanotechnology* **9** 981–985 URL <https://doi.org/10.1038/nnano.2014.216>
- [88] Makhlin Y and Shnirman A 2004 *Phys. Rev. Lett.* **92**(17) 178301 URL <https://link.aps.org/doi/10.1103/PhysRevLett.92.178301>
- [89] Fei J, Hung J T, Koh T S, Shim Y P, Coppersmith S N, Hu X and Friesen M 2015 *Phys. Rev. B* **91**(20) 205434 URL <https://link.aps.org/doi/10.1103/PhysRevB.91.205434>
- [90] Picó-Cortés J and Platero G 2021 *Quantum* **5** 607 URL <https://doi.org/10.22331/q-2021-12-23-607>
- [91] Borhani M and Hu X 2012 *Phys. Rev. B* **85**(12) 125132 URL <https://link.aps.org/doi/10.1103/PhysRevB.85.125132>
- [92] Villavicencio J, Maldonado I, Cota E and Platero G 2013 *Phys. Rev. B* **88**(24) 245305 URL <https://link.aps.org/doi/10.1103/PhysRevB.88.245305>
- [93] Hanson R, Kouwenhoven L P, Petta J R, Tarucha S and Vandersypen L M K 2007 *Rev. Mod. Phys.* **79**(4) 1217–1265 URL <https://link.aps.org/doi/10.1103/RevModPhys.79.1217>
- [94] Goldin Y and Avishai Y 2000 *Phys. Rev. B* **61**(24) 16750–16772 URL <https://link.aps.org/doi/10.1103/PhysRevB.61.16750>